The Star Formation Histories of Disk Galaxies: The Live, the Dead, and the Undead

Augustus Oemler, Jr[1], Louis E. Abramson[2], Michael D. Gladders[3],
Alan Dressler[1], Bianca M. Poggianti[4], and Benedetta Vulcani[5]

[1] The Observatories of the Carnegie Institution for Science, 813 Santa Barbara Street, Pasadena, CA 91101-1292, USA
[2] Department of Physics & Astronomy, UCLA, 430 Portola Plaza, Los Angeles CA 90095-1547, USA
[3] Department of Astronomy & Astrophysics, University of Chicago, Chicago, IL 60637, USA
[4] INAF-Osservatorio Astronomico di Padova, vicolo dell'Osservatorio 5, I-35122 Padova, Italy
[5] School of Physics, The University of Melbourne, VIC 3010, Australia

Abstract

We reexamine the properties of local galaxy populations using published surveys of star formation, structure, and gas content. After recalibrating star formation measures, we are able to reliably measure specific star formation rates well below that of the so-called "main sequence" of star formation versus mass. We find an unexpectedly large population of *quiescent* galaxies with star formation rates intermediate between the main sequence and passive populations and with disproportionately high star formation rates. We demonstrate that a tight main sequence is a natural outcome of most histories of star formation and has little astrophysical significance but that the quiescent population requires additional astrophysics to explain its properties. Using a simple model for disk evolution based on the observed dependence of star formation on gas content in local galaxies, and assuming simple histories of cold gas inflow, we show that the evolution of galaxies away from the main sequence can be attributed to the depletion of gas due to star formation after a cutoff of gas inflow. The quiescent population is composed of galaxies in which the density of disk gas has fallen below a threshold for star formation probably set by disk stability. The evolution of galaxies beyond the quiescent state to gas exhaustion and the end of star formation requires another process, probably wind-driven mass loss. The environmental dependence of the three galaxy populations is consistent with recent numerical modeling, which indicates that cold gas inflows into galaxies are truncated at earlier epochs in denser environments.

Key words: galaxies: evolution – galaxies: fundamental parameters – galaxies: star formation

1. Introduction

That the properties of many galaxies have evolved during recent epochs is a long established fact (Butcher & Oemler 1978, BO78; Madau 1998; Cowie et al. 1996). That the end point of this evolution results in galaxy populations that vary over space has been known for even longer (Hubble 1936, Abell 1965; Dressler 1980, D80). Many processes may contribute to such evolution, of which the most fundamental are internal to the galaxy. Star formation builds structure, so structure will evolve as stars form. Star formation also depletes its own raw material so—unless provided with an unlimited supply of new gas (see Larson et al. 1980, LTC80)—star formation will necessarily drive its own decline and eventual extinction. However, the spatial variation in galaxy populations demands that external effects have significant influence on these processes. It is possible that this influence was exerted during the epoch of formation, setting up those internal properties of the protogalaxy which drove its subsequent evolution (e.g., D80). However, the fact that at least some of the environmental differentiation has occurred at recent epochs (BO78, Dressler et al. 1997; Allington-Smith et al. 1993; McGee et al. 2011) suggests—although it does not require—that much evolution is driven by the continuing interaction of galaxies with their surroundings. Many such processes have been suggested, including shutoff of the external gas supply (LTC80), stripping of gas by a hot external medium (Gunn & Gott 1972), tidal encounters (Richstone & Malumuth 1983; Byrd & Valtonen 1990; Moore et al. 1996), and mergers with other galaxies (Dressler et al. 1999; Struck 2006).

Thus described, understanding galaxy evolution is a choice between galaxy properties set at birth and galaxy properties transformed by later interactions and, if it is the latter, between a number of distinct processes of transformation. Although the causes of the original galaxy properties may remain mysterious, their latter evolution would seem to be a tractable problem. However, the success of the Λ cold dark matter model and the rapid progress in high-resolution modeling of galaxies in formation has shown that the simple choices outlined above are an inadequate description of the actual histories of galaxies. Because the infall of baryons into dark matter halos and the hierarchical merging of these halos is an ongoing process, there are no clear distinctions between galaxy formation and galaxy evolution, or between galaxies and their surroundings. Recent numerical models of galaxy growth have highlighted the involvement of a number of physical processes, including infall of cold and hot gas, heating and possible expulsion of gas by stellar radiation, stellar mass loss, supernovae, shocks, and active galactic nuclei (AGNs), and the transformation of gas content and distribution of stars by mergers. (The literature on this subject is now quite large; good recent summaries include Elahi et al. (2016), with an emphasis on early-type clustered galaxies, and Murante et al. (2014), emphasizing disk galaxies.) Although these models have had increasing success in reproducing some of the observed properties of galaxies, including mass functions, star formation histories, and even metallicities, it is still difficult to reproduce all of the properties of individual galaxies and galaxy populations.

A very different phenomenological approach to the same questions has become quite popular during the last decade, inspired by the discovery of an apparent "main sequence" of

galaxies in the star formation versus mass plane (Noeske et al. 2007). Such a tight correlation between star formation and mass has suggested to some authors (e.g., Dutton et al. 2010; Peng et al. 2010; Sparre et al. 2015; Rodríguez-Puebla et al. 2016; Tacchella et al. 2016) that the myriad of physical processes mentioned above somehow conspire to produce *one* evolutionary track for all galaxies, that track being the main sequence. The majority of galaxies remain on that track even today, but a significant number have been "quenched"; driven off the main sequence by one or more processes, including perhaps such classic mechanisms as stripping, starvation, etc. This idea has an obvious appeal; as is true in stellar astrophysics, the existence of a main sequence might point to a unique set of astrophysics that could bring order to the complicated mess that galaxy astrophysics appears to be. Whatever its appeal, it has yet to be demonstrated that it is correct. In a series of recent papers (Gladders et al. 2013, hereafter G13, Abramson et al. 2015, 2016; Dressler et al. 2016) we have argued for an alternative view. Motivated by the demonstration (Oemler et al. 2013) that many galaxies reached their star formation peaks at recent epochs, we have emphasized the *diversity* of the star formation histories of galaxies. In G13, this diversity was parameterized by log-normal star formation histories with two independent time-scales, corresponding to the epoch of peak star formation and the width of the peak. We have argued that such a description of galaxy histories conforms to the observations at least as well as the main-sequence evolution model, including explaining the existence of the main sequence itself.

We are faced, then, with two sets of questions: how do the many astrophysical processes enumerated above result in the variation with time and environment of galaxy properties, and do these processes lead to a unique path of evolution or to many diverse paths? This is a daunting task, but their recent history should be the easiest aspect of galaxy evolution to understand, for several reasons. With some oversimplification, the complex astrophysics of galaxy formation and evolution can be divided into two rather distinct areas of (1) extrinsic effects that govern the infall of gas into the regions in that stars are forming and (2) intrinsic effects that determine the fate of the gas once it arrives there. Most of the difficulties in the correct modeling of galaxy formation lie in the intrinsic processes. It has been clear since the earliest simulations of forming galaxies in a cold dark matter universe (Navarro & Benz 1991; White & Frenk 1991) that successful models of real galaxies must include massive amounts of thermal and/or mechanical feedback to disrupt infalling cold gas. Models with inadequate feedback inevitably turn too much of the initial baryons into stars, resulting in galaxies that form too fast, are too massive, and are too centrally concentrated. Getting the feedback right has been a difficult task, one that is not yet complete (see Scannapieco 2012, and Elahi et al. 2016, for comparisons of various recent attempts). This difficulty is usually attributed to the inevitably incomplete resolution of small-scale astrophysical processes—such as the interaction of stellar winds and radiation with the very inhomogeneous interstellar medium—which are central to the feedback processes. The extrinsic regime should be less troublesome, since it is dominated by the dynamics of dark matter and of baryons in a much less nonlinear regime than that which occurs within galaxies themselves. At low and moderate redshifts, most galaxies seem to be in a quasi-equilibrium state, with

ordered internal structure and dynamics, and moderate to low levels of star formation. However incomplete our understanding may be of the detailed astrophysics of the intrinsic processes of feedback and star formation, the results of these processes can be observed directly in nearby galaxies in such forms as the Schmidt–Kennicutt law (Schmidt 1959; Kennicutt 1989), which has been shown to govern star formation in a wide variety of galaxies at a range of redshifts (e.g., Daddi et al. 2010; Bouché et al. 2007) and which recent numerical models (e.g., Hopkins et al. 2014) are now able to reproduce with some accuracy. We may be left, then, with only the extrinsic effects as possible variables to explain the recent histories of galaxies.

There is, of course, a very large literature on the systematic properties of nearby galaxy populations. It is well established that there are strong trends present in these populations, including trends of star formation rates with mass, epoch, structure, and environment, of metallicity with mass and galaxy type, and of structure with mass and environment. Also, much work has gone into attempts to delineate the "main sequence" and its evolution with time (Speagle et al. 2014 present a compilation of many of these). Despite all of this work, the subject of local galaxy populations and their implications for galaxy evolution is far from exhausted. In this and subsequent papers, we use multiple published surveys of the local population of galaxies to reexamine the systematic behavior of their main observable properties: mass, star formation rate, disk scale, bulge fraction, and gas content. Our primary goal in this first paper is to understand the present distribution and recent evolution of gas and star formation in disk galaxies. A subsequent paper will examine the issue of bulges and disks. After a careful recalibration of star formation rates, we will show that we can reliably measure star formation rates well below the main sequence and thus follow galaxies as they evolve from the main sequence toward the passive state. We will show that the well-established bimodality in galaxy colors hides an important intermediate population of not-quite-dead galaxies with significant gas but low star formation rates. Delineating the systematic properties of the star-forming, dead, and not-quite-dead galaxies will allow us to put useful new constraints of the processes governing recent galaxy evolution.

The layout of this paper is as follows. In Section 2, we survey the mass–star formation plane, reaching the tentative conclusion that it can be subdivided into three distinct groups: the main sequence, non-star-forming objects, and the intermediate group with low but non-zero star formation rates, which comprises about a third of the galaxy population. In Section 3, we assemble facts about these three populations, deferring most analysis until Section 4, in which we attempt to understand these properties in light of various theories of galaxy evolution. Section 5 summarizes the results. In the Appendix, we will critically examine the star formation rates from Brinchmann et al. (2004) and recalibrate them using the best-available data. This section is critical for establishing the reliability of our detection of low star formation rates, but can be skimmed by those mostly interested in the results.

2. Mapping the Star Formation Rate–Mass Distribution

2.1. Deconstructing the Star Formation Main Sequence

Brinchmann et al. (2004, B04) derived star formation rates from imaging and spectroscopic observations of 149,660 galaxies from DR2 of the Sloan Digital Sky Survey (York et al. 2000), which have spectroscopic observations,
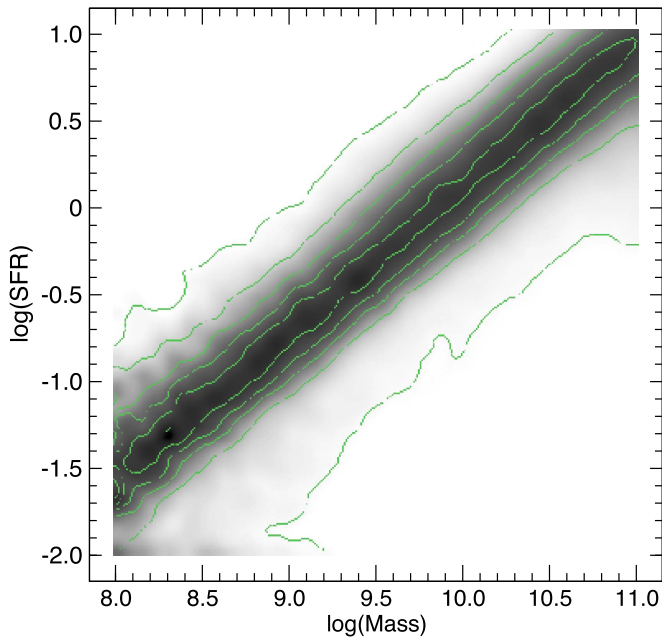
Figure 1. Density of galaxies in the log(SFR)–log(mass) plane, for the sample of B04 galaxies analyzed by P10. The contours represent equal normalized density intervals.

Figure 2. sSFR vs. mass relation for the entire B04-DR7 sample, using the sSFR values derived in the Appendix. Superimposed are the median completeness limits at, from left to right, the first through third quartiles of the redshift distribution of the galaxies.

r magnitudes in the range $14.5 < r < 17.77$, and redshifts between 0.005 and 0.22. They also incorporate mass determinations from Kauffmann et al. (2003). In 2007 they recalibrated their method and applied it to the DR7 release. These new data are not published but are available on the web.[6] We will use this latter data set, which we denote as B04-DR7, in all of the following analysis. The mass values we shall use as given; all determinations of galaxy stellar masses are derived from SED data using stellar population models and we have no reason to think that we can improve on those of Kauffmann et al. Any significant errors are probably systematic to the population model and will only shift the mass scale, which should not affect our analysis. There are, however, independent methods of determining star formation rates and in the Appendix we use what we believe are the best of these to improve on the B04-DR7 SFRs. Starting with the best-available SFRs derived from hydrogen recombination lines, we calibrate an SFR indicator based on mid-IR plus near-UV photometry. Using this indicator, we derive mean corrections to the BO4-DR7 SFRs. These still show significant scatter at low SFRs, but by averaging these with SFR values derived from near-UV to optical colors, we obtain SFRs that agree well with the UV–IR values down to values of log(sSFR) = log(SFR/mass) ∼ −12. The main changes are to the star formation rates of galaxies with weak or undetected emission lines. Unless otherwise noted, all quoted SFR values are based on our recalibration.

First, though, we begin with the original B04 data. A particularly striking presentation of the star-forming main sequence to be found in the B04 data is presented in Figure 1 of Peng et al. (2010, P10). We repeat this presentation of the B04 data in Figure 1. The density of objects is normalized so that the integrated density per interval of log mass is constant, which permits a better appreciation of the behavior of star formation as a function of mass. This is a quite striking correlation, with a scatter $\sigma(\log(\text{SFR})) \sim 0.29$. If, as has often
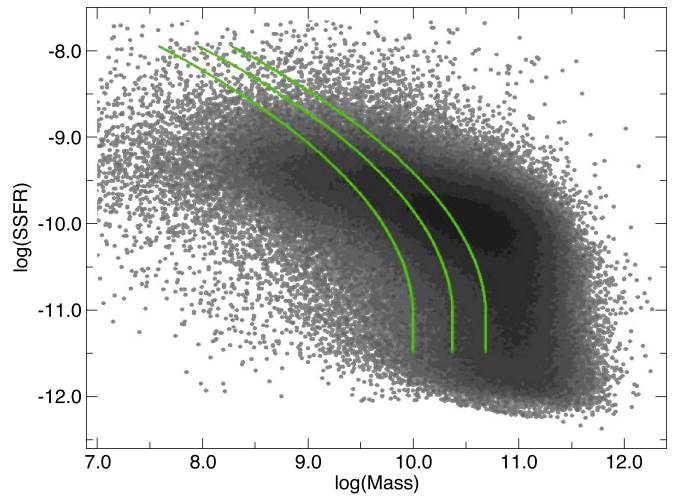
---

been assumed (but we show in the Appendix to be incorrect), the typical errors in B04 star formation rates were as large as 0.2–0.3 dex, Figure 1 would seem to imply that the true scatter in the star-forming main sequence is quite small.

Unfortunately, this plot does not stand up to close scrutiny. The first thing to note is that plotting observed SFR versus stellar mass gives a quite misleading impression of the correlation between these quantities, because the stellar mass is simply the time integral of the star formation rate. More precisely,

$$M_{\text{tot}} = \int_0^{t_0} \text{SFR}(t) f_l \, dt = f_l t_0 \langle \text{SFR} \rangle, \tag{1}$$

where f_l is the fraction of the mass that remains locked up in stars rather than returning to the ISM during stellar evolution. Unless $\langle \text{SFR} \rangle$ is completely uncorrelated with SFR(t_0)—which would imply a completely random history of star formation—SFR will *always* be correlated with mass, whatever the underlying astrophysics or history of star formation. A less misleading presentation of the B04 data can be obtained by plotting *specific* star formation rate, sSFR = SFR/M_{tot} versus mass. We can write sSFR as

$$\text{sSFR}(t) = \frac{1}{f_l t} \frac{\text{SFR}(t)}{\langle \text{SFR} \rangle}. \tag{2}$$

Thus, sSFR is an (incomplete) measure of the star formation history of a galaxy in that, while many histories can lead to the same forms of sSFR(t), different values of sSFR(t) require different histories.

Also, we must improve on the data set used in Figure 1. First, we replace the B04 star formation rates with those obtained in the Appendix, which are more accurate, particularly for low star formation rates. Second, P10 culled their galaxy set in two problematic ways: by excluding galaxies without strong emission lines or with some sign of an AGN component and by excluding galaxies without sufficiently blue $U - B$ colors. All of these exclusions will narrow the sSFR range. The result of these corrections is presented in Figure 2 where we now plot the sSFR–log(mass) distribution for all objects with detected
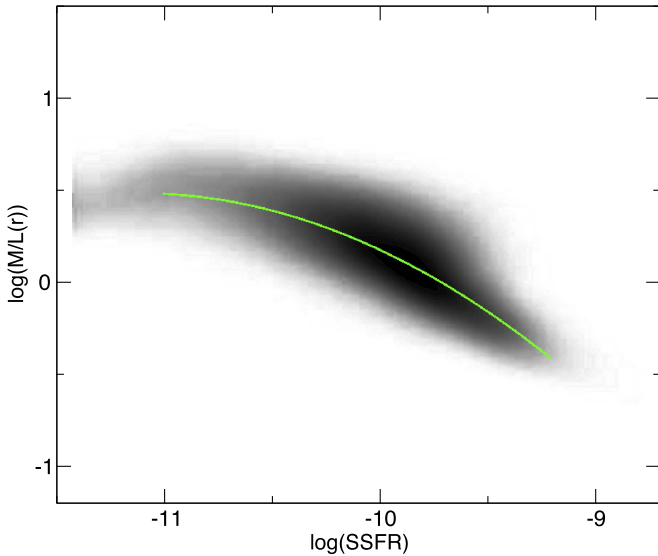
Figure 3. *r*-band mass to light rations of the B04 sample vs. sSFR. The green line is the adapted median relation.

Figure 4. sSFR vs. mass for the maximally complete sample.

Figure 5. Distribution of log(sSFR) for galaxies in the maximally complete sample, in three narrow intervals of log(mass), centered at 9.5 (blue), 10.0 (black), and 10.5 (red).

star formation (i.e., $\log \mathrm{sSFR} > -12.2$). (We now plot individual points rather than a normalized distribution.)

This distribution is obviously much broader than that in Figure 1, but one source of bias remains. The analyses of B04 and P10, as well as those presented so far in this paper, have included all sample galaxies (of particular spectral properties) at every redshift. The SDSS spectroscopic sample is complete to $r = 17.8$. To see what this means for mass completeness we must consider the mass-to-light ratios of the galaxies. In Figure 3, we plot the distribution of *r*-band mass to light ratios of the B04-DR7 galaxies versus their sSFR and fit a polynomial to the median value of $M/L(r)$ versus log(sSFR), over the sSFR range $-11.5 \leqslant \log(\mathrm{sSFR}) \leqslant -9.2$ where most of our objects lie. Superimposed on the sSFR–mass distribution in Figure 2 are the mass limits derived using that polynomial fit at the first through third quartiles of the redshift distribution of the sample, namely $z = 0.054, 0.083, 0.119$. The sample is more than 50% incomplete to the left of each line. Clearly, the data as usually presented are seriously incomplete. Furthermore, because of the slope of the completeness lines, galaxies with lower sSFRs are systematically excluded since they are less luminous at a given mass than those with high sSFRs. Note that this effect operates at every mass, since the higher mass galaxies are drawn preferentially from higher redshifts.

Given the results in Figures 2 and 3, we can construct the largest complete sample of B04-DR7, which we denote the *maximally complete sample* by, at every mass, including only galaxies out to a redshift such that all galaxies with $\log(M/L(r)) \leqslant 0.8$, the maximum found in the sample, will have $r \leqslant 17.8$ and therefore will be included in the complete SDSS spectroscopic sample. In order to minimize the mismatch between galaxy size and SDSS fiber size, we also limit the sample to objects with $z \geqslant 0.01$. Note that this sample, although unbiased in star formation properties at each mass, is strongly biased toward high mass, since the sample of higher mass objects is complete over larger volumes.

The results for this sample are presented in Figure 4. The beautifully clean star-forming main sequence of Figure 1 has almost disappeared. Although some sort of sequence is apparent at low mass, it seems to be entirely obscured at high
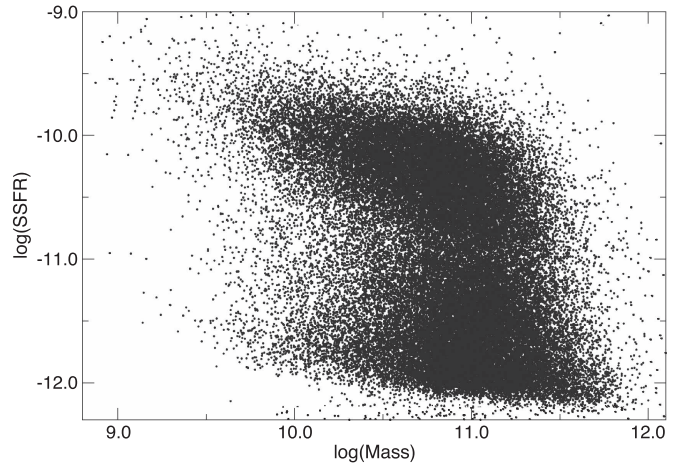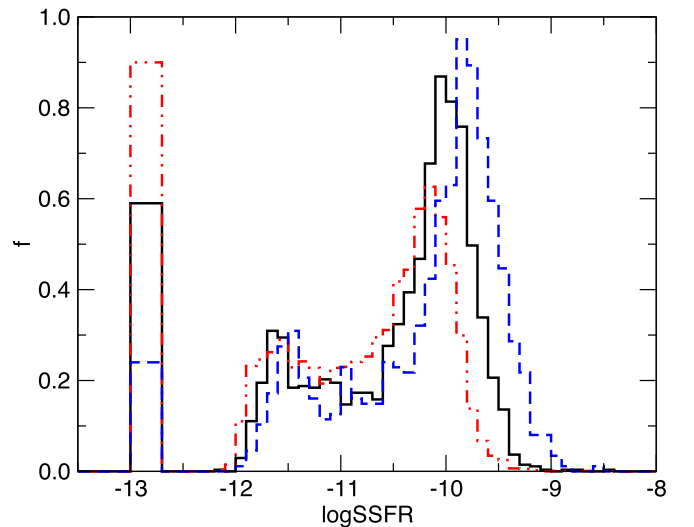
masses by a broad swath of lower SFR objects. In all following analyses, the sample will be limited to the maximally complete sample unless explicitly stated otherwise.

2.2. Repopulating The Mass–Star Formation Plane

Figure 4 shows that the sSFR–mass distribution is very broad, with a distinct narrow main sequence only apparent at low masses (log(mass) < 9.5). However, closer examination shows that this broad distribution has significant structure. Figure 5 presents the distribution of sSFR in three intervals of log(mass): 9.3–9.7, 9.8–10.2, and 10.3–10.7. Three peaks are apparent in all of these: one for those without detectable star formation—which we arbitrarily place at log(sSFR) = -12.8, one at log(sSFR) ~ 11, and one at log(sSFR) ~ 10. The middle peak is broad and does not shift with mass, but the upper peak is narrow, and moves to lower values of log(sSFR) as mass increases. It is reasonable to still call the upper peak the "main sequence." Using all objects with log(sSFR) > log(sSFR)$_{\mathrm{peak}}$ − 0.5, we obtain the dispersion of the main sequence—σ(log(sSFR)) = 0.30, independent of mass, as well as its slope d(log(sSFR$_{\mathrm{peak}}$))/d(log mass) = -0.43. It should be noted that the width of the main sequence, though narrow, is
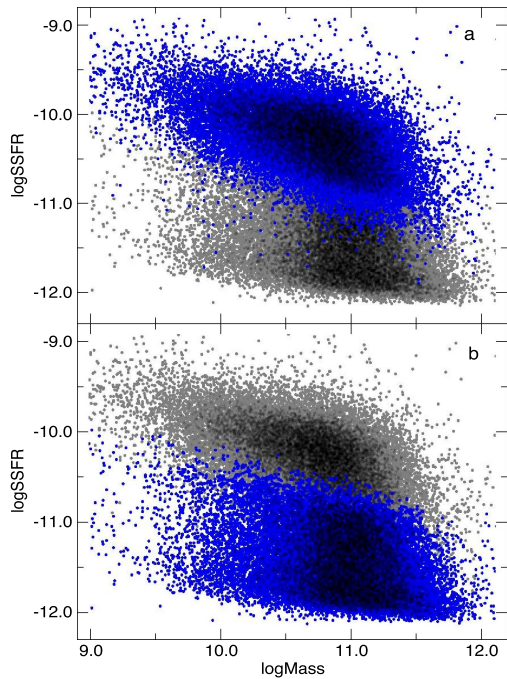
Figure 6. Decomposition of the maximally complete sample of star-forming galaxies into main-sequence galaxies and others. In (a) the main-sequence objects are shown in blue and overlay the others, in (b) the order is reversed.

real, since the scatter in our best sSFR measure, established in the Appendix, is substantially less than 0.3dex at the main sequence.

Let us assume for the moment that the main sequence is a distinct component of the sSFR–mass distribution, separate from the intermediate sSFR group, with the shape described above. If we also assume that the main sequence dominates the distribution at values of log(sSFR) higher than the main-sequence peak, and that the distribution is symmetrical about the peak, we can use counts of objects with sSFR > sSFR$_{peak}$ to obtain its mass function, and using that plus the slope and spread, we can generate the entire main sequence and statistically remove it from the sSFR–mass distribution of all galaxies. The results of this decomposition—ignoring the dead galaxies with no detectable star formation—are presented in Figure 6. The most striking implication of this decomposition is that the main sequence, rather than dominating the sSFR–mass plane, as implied by, for example, Figure 1, only contains about half of the star-forming galaxies. The other half belong in a broad swath stretching from below the main sequence down the the level at which star formation becomes undetectable.

The existence of a population of galaxies with star formation rates significantly lower than the main sequence is not a new discovery, but it has not received much attention. It is absent from color distributions, which only show the main sequence and no-star formation peaks and an almost empty "green valley," because galaxy colors are insensitive to sSFR values below about log(sSFR) ∼ −11 (see Dressler & Abramson 2015). Such a population is apparent in Figure 24 of B04, as well as in Figure 22 of Salim et al. (2007). Schiminovich et al. (2010) discussed it in relation to star formation efficiency (to which we will turn in Section 3.3), and Tojeiro et al. (2013) in relation to star formation histories. In most cases its importance has been underestimated because of the sample bias described by Figure 2, as well as by the difficulty in calibrating very low star formation rates. The most explicit recognition of this

phenomenon was by Eales et al. (2017, E17), who constructed a volume-limited sample of 323 nearby galaxies and derived star formation rates and masses from multi-band photometry. Their Figure 2 is very similar to our Figure 4 over the mass range that we have in common. (They report sSFR values to much lower levels than we have ventured to do, but the fraction of objects with log(sSFR) < −12 is similar in the two studies.)

SDSS images (York et al. 2000; Albareti et al. 2017) of a random subset of these low sSFR galaxies are presented in Figure 7. Most appear to be rather normal early-type galaxies. A set of 51 galaxies in the low star formation group that are members of the Coma Cluster and were classified by D80 contains only 4 that were not typed as normal Es or S0s, including 1 Ep, 2 S0/a's, and 1 Sb.

The identification of the low sSFR subset of galaxies as a distinct component is only a convenient working hypothesis, although the distributions in Figure 5 give some credibility to the idea. Also, the distinction between these objects and those with no detected star formation is presumably an artifact of our inability to measure specific star formation rates below log (sSFR) = −12. Nevertheless, for the moment we will divide the galaxy population into three distinct groups: those with vigorous star formation, which we will continue to call the *main sequence*, the intermediate group, which we will denote as *quiescent*, and those with no detected star formation, which we will call *passive*. For the following analysis, we will label galaxies as "main sequence" or as "quiescent" according to their assignment in the statistical decomposition presented in Figure 6. In the overlap region this is, of course, an arbitrary assignment, but no more arbitrary that doing the cut at some specified value of sSFR. All objects below the detection limit of log(sSFR) = −12.2 are classified as "passive." In coming sections, we will explore how the properties of these populations are related to their gas content, environment, and structure.

3. Properties of the Three Populations of Galaxies

3.1. Environmental Dependence

In Figure 8 we present the incidence of our three star formation classes as a function of environment, in five mass ranges, using two measures of environment. We take these measures from Tempel et al. (2012) who, as part of a clustering survey of SDSS DR8 galaxies, determined group membership and normalized galaxy densities within 1, 2, 4, 8, and 16 Mpc of a sample of SDSS galaxies, which includes about 89% of our maximally complete sample; we will use their group membership, as well as the density within 1 Mpc, which we denote as $\rho_{1.0}$. Errors for points in the left column are typically 0.01, those in the right column range from 0.005 for small N_{group} to 0.02 for $N_{group} > 100$. It is clear that star formation is sensitive to environment at every mass and in every environment, though high-mass galaxies show a lower sensitivity than do low-mass ones. Conversely, in every environment, high-mass galaxies are more likely to be quiescent or passive than are low-mass objects. At first glance, the population of quiescent galaxies appears to be quite stable, with only the ratio of star-forming to passive galaxies varying with environment, but this appearance is misleading. In Figure 9 we plot, for every data point in Figure 8, the fraction of main-sequence galaxies versus the ratio of quiescent to passive galaxies. The result shows that

Figure 7. SDSS images of a representative sample of brighter galaxies with log(sSFR) ∼ −11.5. Each image is 48″ across.
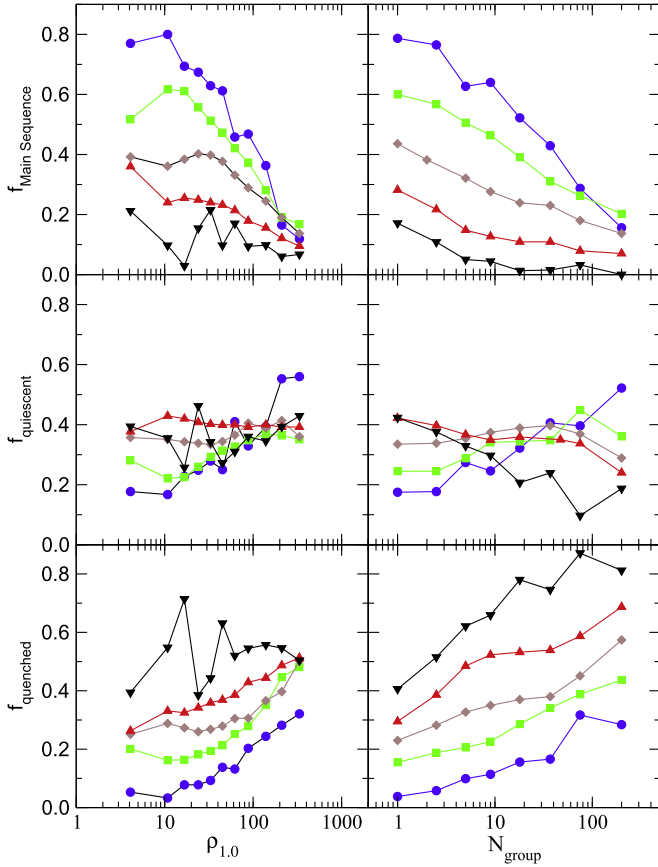

Figure 8. Variation of fractions of the three galaxy types with environment, in 5 ranges of log(mass); blue circles: 9.5–10.0, green squares: 10.0–10.5, brown diamonds: 10.5–11.0, red up triangles: 11.0–11.5, black down triangles: 11.5–12.0. Left column—galaxy populations vs. galaxy density within 1 Mpc; right column—populations vs. group membership. Top row—fraction of main-sequence objects, middle row—fraction of quiescent objects, bottom row—fraction of passive objects.
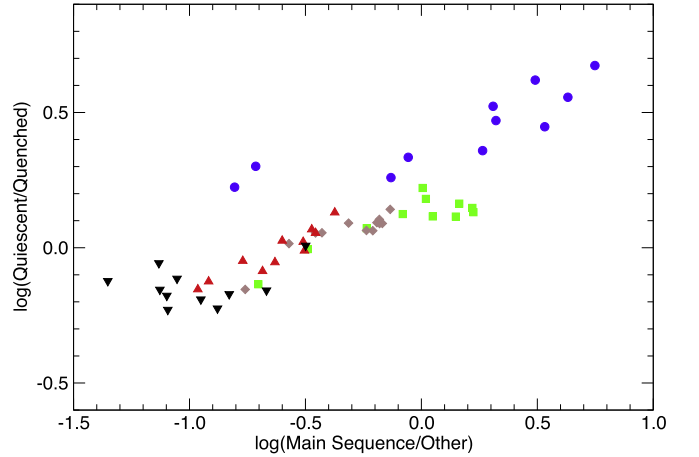

Figure 9. Fraction of main-sequence galaxies vs. the ratio of quiescent to passive galaxies for each data point in Figure 8. Points are labeled by mass range as in Figure 8: blue circles: 9.5–10.0, green squares: 10.0–10.5, brown diamonds: 10.5–11.0, red up triangles: 11.0–11.5, black down triangles: 11.5–12.0.

there is a very strong correlation between these two quantities at every mass and local density. The lower the fraction of main-sequence galaxies, the lower the fraction of galaxies below the main sequence with some star formation.

3.2. Gas Content

Two H I surveys cover large portions of the volume of the B04-DR7 sample. The ALFALFA survey (Giovanelli et al. 2005, Haynes et al. 2011) used the Arecibo Telescope for a blind survey of a significant fraction of the North Galactic Cap over the velocity interval $1600 \, \mathrm{km \, s^{-1}} \leqslant cz \leqslant 18000 \, \mathrm{km \, s^{-1}}$. The survey volume included about 3×10^4 B04-DR7 galaxies (1×10^4 in the maximally complete sample), of which about
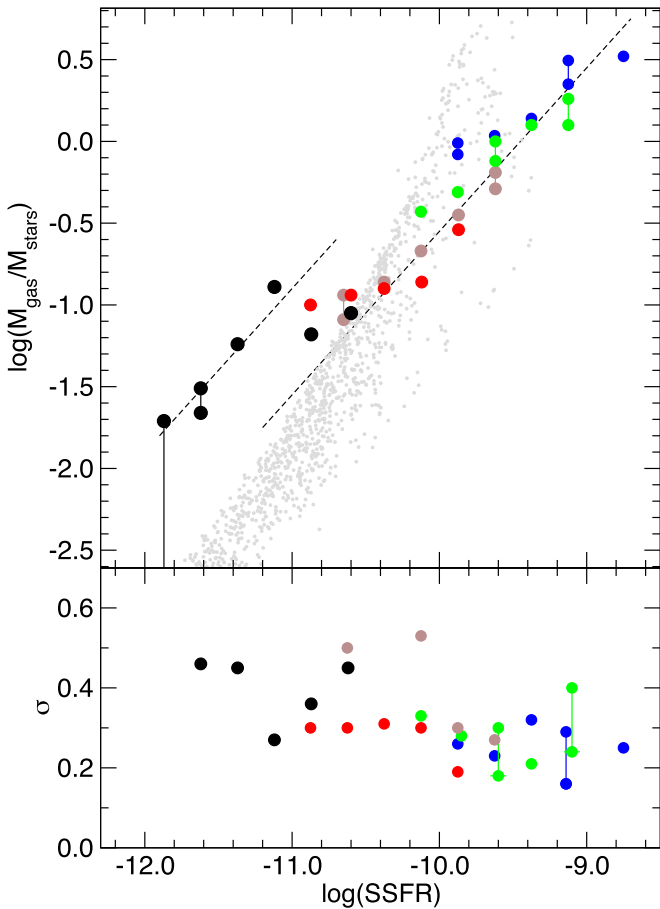
Figure 10. H I gas content per unit mass vs. sSFR. a—median gas content, b—1σ dispersion about the median. Black circles—GASS+ALFALFA sample, colored circles—ALFALFA sample in four ranges of log(mass): blue—9.0–9.5, green—9.5–10.0, brown—10.0–10.5, red—10.5–11.0. Upper dashed line—$\tau_{gas} = 21 \times 10^9$ years, lower dashed line—$\tau_{gas} = 4.7 \times 10^9$ years, gray points—log-normal model galaxies from G13.

9×10^3 were detected (3×10^3 in the maximally complete sample). The sensitivity of the survey varies with linewidth, but a typical limit for 50% completeness is $\log(M_{H I}) = 12.63 + 2\log(z)$, or $5 \times 10^9 M_\odot$ at the median redshift of the survey. The GASS survey (Catinella et al. 2010, 2012) is a pointed survey of about 10^3 galaxies within the ALFALFA survey volume, which were *not* detected either by ALFALFA or by Springob et al. (2005). It includes only objects in the mass range $10.0 \leqslant \log(\text{mass}) \leqslant 11.2$, and the redshift range $0.025 \leqslant z \leqslant 0.05$. It is about a factor of five deeper than ALFALFA at the same redshift.

Figure 10 summarizes the H I content of the B04-DR7 galaxies derived from these two surveys. Figure 10(a) plots the median gas to stellar mass ratio as a function of log(sSFR), in intervals of galaxy mass, and Figure 10(b) plots the 1σ dispersion, calculated from the difference between the 50th and 84th percentiles of the distribution. Above log (sSFR) = −11.0 the ALFALFA survey detected the majority of the galaxies over some subset of the survey volume, allowing a determination of both quantities. Since the survey is approximately flux-limited, the detection rate is a function of $M_{gas}z^{-2} = M_{stars}(M_{gas}/M_{stars})z^{-2}$. The redshift limit of each M_{stars} and sSFR subset is chosen to sample as large as possible a fraction of the ALFALFA volume, while still reaching deep enough into the M_{gas}/M_{stars} distribution to allow determination

of the median value. Since the detection threshold is rather broad, there will be some detections below the completeness limit and some non-detections above the limit. We handle non-detections in two ways (1) by assigning them a value of M_{gas}/M_{stars} equal to the 50% completeness limit or by assigning them values of zero. Where these differ, both points are plotted. When the majority of the objects are undetected, the latter value goes to zero, as with the leftmost black point in Figure 10(a). The ALFALFA results are presented in Figure 10 as colored points, divided into the same mass intervals as in Figure 8. Errors in the ALFALFA sample range from 0.02 to 0.04 for median values of $\log(M_{gas}/M_{stars})$, and from 0.015 to 0.035 for σ.

Below $\log(\text{sSFR}) = -11.0$, the ALFALFA sample in insufficiently deep and we turn to the GASS survey. Here things become slightly complicated. The GASS sample is a random subset of objects within the ALFALFA survey volume with redshifts $0.025 \leqslant z < 0.05$ and masses $10.0 \leqslant \log(\text{mass}) < 11.2$, but excluding objects that were already detected by ALFALFA. Because the GASS sample itself is does not contain objects already detected in ALFALFA, we account for the missing objects in a way similar to that applied by Catinella et al. (2010). The GASS sample objects are (almost) all contained within our B04 Maximally Complete Sample, which we abbreviate MAXSAMP. Let S_A be the subset of ALFALFA objects in MAXSAMP and within the GASS mass and z ranges. Let S_G be the subset of GASS objects within MAXSAMP. Since the ALFALFA detection probability within S_A will depend on the galaxy mass, we divide the sample into mass intervals. Then, it is straightforward to show that in each interval, if $\tilde{A}$ is the number of *undetected* S_A objects and G is the total number of S_G objects, we can combine the GASS objects with the ALFALFA detected objects by giving each S_A detection a weight of $G/\tilde{A}$. The GASS sample is too small to subdivide by mass, so we include all objects. We deal with GASS non-detections in the same manner as with the ALFALFA sample. The results are presented in Figure 10 as black points. Typical errors in the GASS sample are about 0.08 for the median values of $\log(M_{gas}/M_{stars})$ and 0.06 for values of σ.

The diagonal dashed lines are lines of constant gas-to-star formation rate, which is, to within a factor of f_l, the inverse of gas consumption timescale, τ_{gas}. The upper line corresponds to $\tau_{gas} = 21$ Gyr and the lower line to $\tau_{gas} = 4.7$ Gyr. Several points seem clear. (1) At a given sSFR, the scatter in gas to stellar mass ratio is rather small, no more than a factor of two. (2) Gas consumption timescales seem to be independent of galaxy mass. (3) The trend of gas content with sSFR is not inconsistent with a simple picture in which the median gas consumption timescale of main-sequence galaxies is 4.7 Gyr, independent of sSFR, and the median gas consumption timescale of quiescent galaxies is 21 Gyr, independent of sSFR.

Another view of the gas consumption issues is illustrated by the gray points. In Gladders G13, we constructed models for the star formation histories of galaxies with log-normal shapes of the form

$$\text{SFR}(t) = S_0 \frac{1}{t\tau\sqrt{2\pi}} e^{-(\ln t - \ln(t_0))^2 / 2\tau^2}, \qquad (3)$$

fitting the distribution of shape parameters using observations of low- and high-redshift galaxy populations as constraints. If galaxies were closed boxes, with gas neither entering nor
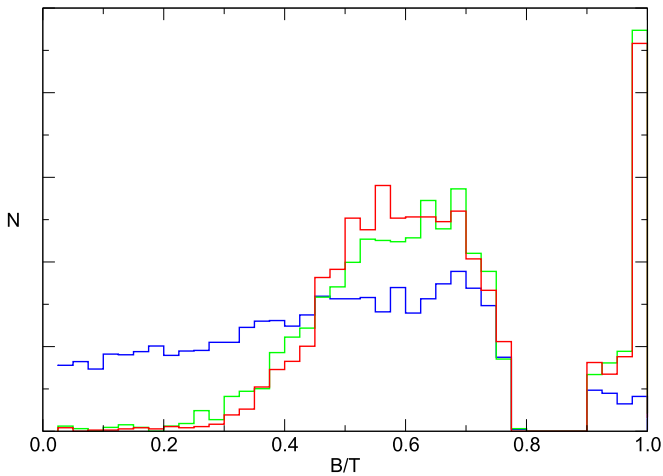
Figure 11. Distribution of bulge mass fraction for star-forming—blue, quiescent—green, and passive-red galaxies, in the mass range $10.0 \leqslant \log (\text{mass}) < 11.0$.

leaving, and if all gas was eventually turned into stars, then a galaxy's gas content at any time would be just that needed to form the mass of stars it will form in its future. Since we know the future evolution of each G13 galaxy, we can determine the gas–sSFR distribution of those galaxies. (To convert the total gas content that the models consider to the H I content that the ALFALFA and GASS surveys provide, we use the median value $\log(M\,\text{H2}/M\,\text{H I}) \sim -0.5$ implied by Figure 9 of Saintonge et al. 2011.) The results are presented as gray points in Figure 10. The important point is that the median of the gray points lies near or above the median gas content of main-sequence galaxies, but well below that of the quiescent objects. Thus, the median gas content is more than sufficient to fuel the future star formation of all of the quiescent galaxies, but not all main-sequence objects. These models represent only one possible description of galaxy formation histories, though they do fit well all of the extant constraints. However, it is likely that most alternate models, or at least those in which star formation decreases steadily from a peak at early times, will have a qualitatively similar distribution. Therefore, it appears that many (though far from all) main-sequence galaxies will require a continuing inflow of gas to maintain their star formation, as pointed out long ago by LTC80, but that quiescent galaxies do not. We will consider the implications of this fact in Section 4.

3.3. Galaxy Structure

We close this section with a brief look at galaxy bulges and disks. We shall examine this in much greater detail in a subsequent paper, but one important fact will be useful in the following discussion. It has long been known (Hubble 1926; Baade 1951) that the masses, stellar populations, and structures of galaxies are correlated: high mass, bulge-domination, and low star formation rates tend to be associated with each other, as are low mass, disk-domination, and high SFR. Mendel et al. (2014) determined the masses of disks and bulges for a large fraction of the B04-DR7 set of galaxies. In Figure 11, we compare the bulge mass fractions (which we will designate B/T) of the three galactic populations with masses in the range $10.0 \leqslant \log (\text{mass}) < 11.0$. To avoid the ambiguous overlap region near $\log (\text{sSFR}) \sim -10.75$ we only take main-sequence galaxies with

$\log(\text{sSFR} > -10.5)$ and quiescent galaxies with $\log (\text{sSFR}) < -11.0$. The import of this figure is clear: quiescent and passive galaxies are structurally almost identical and very different from the star-forming population. While star-forming galaxies have an almost uniform distribution of bulge mass fraction, there are almost no disk-dominated quiescent or passive galaxies, those with bulge mass fractions less than 0.2. Conversely, there are very few bulge-dominated ($B/T > 0.9$) star-forming galaxies. Much but not all of this is old news: it is a commonplace that there are very few star-forming ellipticals, and the lack of disk-dominated S0s was first noted by Sandage & Visvanathan (1978), who argued from this that S0s could not be stripped spirals (more on this later.)

4. Discussion

4.1. The Physical Significance of the Main Sequence

Multiple lines of evidence seem to suggest that main-sequence and quiescent galaxies form distinct populations. The evidence includes the sSFR distribution at fixed mass (Figure 5), the variation in the incidence of the populations with environment (Figures 8), the sSFR dependence of gas content (Figure 10), and the almost total absence of pure disk galaxies among the quiescent and passive populations (Figure 11). That the main sequence is a physically distinct population has been a common theme of many recent papers, many of which have tried to identify the astrophysical processes responsible for the tight SFR versus mass dependence. The above list seems to support such a view, but the existence of a well-defined population does not necessarily imply a physical process driving the SFR–mass correlation. As was noted in Section 2, *any* star formation histories that are not completely random will produce a correlation of SFR with mass. As Equation (2) makes clear, the peak of the resulting sSFR distribution will be determined only by the age of galaxies (t_0) and the mean value of $\text{SFR}(t)/\langle\text{SFR}\rangle$. If the majority of galaxies are of comparable age, then only the range of the shapes of the star formation histories will produce a scatter in sSFR.

Two very general considerations require that the sSFR distribution fall rather rapidly away from the peak. Equation (2) constrains the high side. If we assume that very few galaxies have rising star formation rates at the present epoch, Equation (2) requires that the sSFR distribution fall fast at high values of sSFR, nearing zero at $\text{sSFR}(t) = 1/ft_0$. Similar considerations constrain the low side. At early times—shorter than the timescale over which SFR varies—$\text{SFR}(t) \approx \langle\text{SFR}\rangle$ for all galaxies. Therefore, if star formation rates are now falling and if $d^2\text{SFR}/dt^2$ is zero or negative, the galaxies with the lowest values of sSFR today will be those in which SFR has fallen the fastest. If lower sSFR galaxies evolve faster, then galaxies accelerate away from the "main sequence," traversing each successive interval of sSFR more quickly, resulting in a decreasing density of objects at lower sSFR. Note that these effects depend not at all on any particular assumptions about the physical processes driving the star formation history.

As an illustration of this effect, we construct a random population of galaxies based on the log-normal star formation histories of the form described by Equation (3), developed in G13. In that paper, the distribution of the parameters t_0 and τ were tuned to match observations of the history of the star formation density as well as of the sSFR distribution. Here we
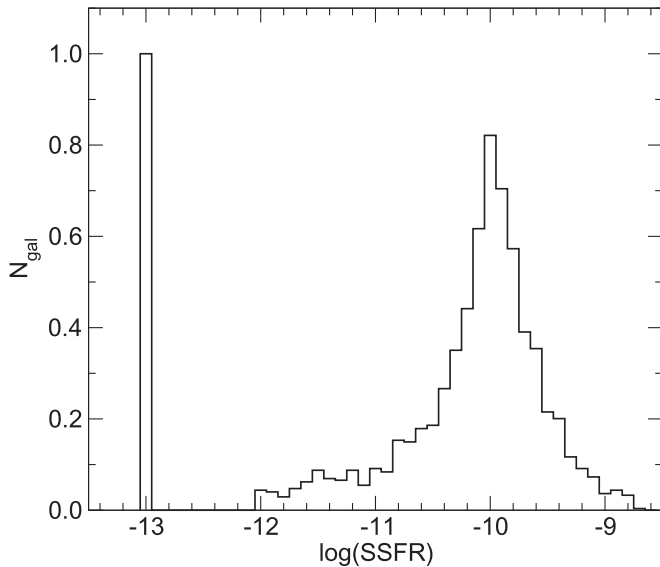
Figure 12. sSFR distribution of galaxies at the present epoch, from a simulation of log-normal star formation histories in which the two parameters of the log normal are distributed at random over the range $1.5 \leqslant t_0 < 20$ Gyr, $0.1 \leqslant \tau < 1.1$.

take a completely random set of values over the range 1.5 Gyr $\leqslant t_0 < 20$ Gyr, $0.1 \leqslant \tau < 1.1$, considerably broader than what was needed to fit the observed sSFR distributions. We evolve the histories until the present age of the universe and calculate the present epoch sSFR of each object. Values of log (sSFR) < -12 are assumed to be undetectable and are set to the arbitrary value of -13. The results are presented in Figure 12; from the 16th and 84th percentiles of the distribution of detected objects we calculate $\sigma(\log(\mathrm{sSFR})) = 0.36$, only slightly broader than we have determined for the real "main sequence" in Section 2. Thus, a completely random set of star formation histories produces an sSFR distribution almost identical to that observed. The point is that the existence of a "main sequence" signifies little about the history of the star formation in a galaxy population. We have chosen a log-normal form for illustration, but virtually any set of star formation histories satisfying the two constraints that (1) $d^2\mathrm{SFR}/dt^2$ is zero or negative and (2) star formation histories are smooth rather than having large random excursions (which could temporarily push sSFR to arbitrarily high or low values) will produce a similar distribution. From Equation (2), we expect the peak to be located somewhat lower than $1/t$, which means that it will rise with increasing redshift, as it is observed to do. Therefore, the attempt to construct physical models to explain the properties of the main sequence is misguided. Although it is possible that some detailed astrophysical considerations could duplicate the behavior that we have seen to occur naturally, simplicity demands that we accept the straightforward explanation described above, until some new information forces us to look for elsewhere.

4.2. The Physical Significance of the Quiescent Galaxies

If the main sequence is a natural consequence of the age of galaxies and a smooth evolution of their star formation rates, the same is not true of the quiescent population. Figure 12 and the preceding argument both show that there should be a rapidly falling tail of the sSFR distribution to the low side of the main-sequence peak, rather than the large population of

galaxies at low sSFR values that are observed. Although the existence of a population of intermediate sSFR galaxies is not news, many of the properties of this population are new, and are quite puzzling, so we should first address the possibility that our low sSFR galaxies are spurious and are the result of errors in the star formation rates. We demonstrated in the Appendix, by a comparison with star formation rates derived from (mostly independent) UV+IR measures, that our SFR measure is quite accurate, but the possibility remains that *all* of the star formation measures are systematically wrong.

It is easy to rule out the possibility that the sSFR values of the quiescent objects are spuriously low, i.e., that they are misclassified main-sequence objects. Neither their appearance (Figure 7), dependence on mass and environment (Figure 8), gas content (Figure 10), or structure (Figure 11) look anything like that of the main sequence. At most, only a very small fraction of the quiescent class could be misclassified main-sequence objects. Might they be misclassified passive objects? Many of their properties are closer to passive than to main-sequence galaxies. However, their dependence on mass and environment are quite different (Figure 8), as is their gas content. In a sample of quiescent and passive galaxies within the ALFALFA survey volume, matched in redshift and mass distribution, H I gas is detected in 10.3% of the quiescent galaxies but only 1.7% of the passive objects. In similarly defined samples from the GASS survey, the fractions are 57% and 16%. This is inconsistent with the quiescent objects being drawn from the passive population (but suggests, as one would expect, that some fraction of the objects in the passive class might be very low sSFR quiescent galaxies). Also, E17 have derived a very similar distribution of sSFR values, using a derivation of star formation rates that is very different than ours.

We conclude, therefore, that the great majority of the quiescent galaxies are correctly typed and the results summarized above cannot be dismissed as being due to SFR measurement errors. That said, we do *not* claim that the quiescent and passive objects form separate populations. The dividing line between the two is set purely by the considerations described in the Appendix: below $\log(\mathrm{sSFR}) = -12.2$ we cannot reliably detect star formation in our sample galaxies. It is likely that the two groups form one continuous population differing only quantitatively in their sSFR values. Whether there is a distinct group of galaxies with absolutely no star formation is far beyond our ability to determine.

To understand the quiescent galaxies, we need a model of galaxy evolution with more content than the random assemblages of log normals used earlier. However, we do not need a full-blown numerical simulation; a toy model of galaxy formation based on the considerations mentioned in Section 1 will suffice. As we pointed out earlier, galaxy evolution divides, roughly, into intrinsic and extrinsic effects. The intrinsic effects are very complicated, but they result in star-forming behavior that at recent times has been directly observed and characterized, i.e., the Schmidt–Kennicutt Law. Extrinsic effects are not, in general, observable and—absent a full numerical model—are not calculable. We have no such model and no completely successful model has yet been constructed. However, if we ignore mergers, the result of these extrinsic processes is to deliver a net amount (infall–outflow) of *cold* gas to the star-forming regions of the galaxy with some unknown time dependence. Here we adapt the simplest

possible such history: a constant rate of addition, which begins at time $t_0 \geqslant 10^8$ years and continues until a time $t_0 < t_1 \leqslant 13.67 \times 10^9$ years. We assume the the gas flows into the disk with a radial density profile like that of the stars in disks today $\rho_{gas} \sim e^{-r/r_0}$. From the data of Simard et al. (2011) we obtain mean values $r_0 = 2.66\sqrt{M_{gal}/10^{10}}$ and a dispersion of about a factor of 2.0. We take the parameters of the Schmidt–Kennicutt Law from Kennicutt (1998)—more recent compilations (e.g, Daddi et al. 2010) are still consistent with these values—which can be expressed as $\Sigma_{SFR} = 1.5 \times 10^{-10}\Sigma_{gas}^{1.4}$, where Σ_{SFR} is the surface density of star formation in solar masses per year per square parsec and Σ_{gas} is the surface density of gas in solar masses per square parsec.

This model cannot deal with bulge formation, but it need not do so. Whether bulges are formed very early in galactic history, or present day bulges are the result of the last major merger between previous disk galaxies, the history of the *present* disk likely only begins after bulge formation is complete. After that time, the bulge contributes mass but neither gas nor star formation. Since the typical galaxy in our mass range has a bulge mass fraction of about 0.5, we account for the bulge by shifting both the gas-to-mass ratio and the specific star formation rate of our model galaxies down by a factor of two.

This model is only a toy but should not be a bad descriptor of at least the recent evolutionary history of the stellar populations of galaxies. Different infall histories or starbursts may change the short-term star-forming behavior, but will have little long-term effect. In Figure 13, we compare the predictions of this model for sSFR distribution and gas content with the observations reported earlier, for galaxies in the mass range $10.0 \leqslant \log$ mass) < 11.0. To convert the total gas content required for the Schmidt–Kennicutt law with the observed H I content we again us the value $\log(M\,H2/M\,H\,I) \sim -0.5$ from Saintonge et al. (2011). The agreement is not good. The model reproduces, roughly, the sSFR distribution and gas content of the main sequence, but fails completely at lower values of sSFR, producing neither quiescent nor passive galaxies.

However, our description of the star formation dependence on gas content is not yet complete. Kennicutt (1989) and Martin & Kennicutt (2001) demonstrated that, below a critical density—probably related to the local Toomre Q disk stability threshold (Toomre 1964)—star formation rates fall precipitously. If the Q parameter is indeed the governing factor then, for a flat rotation curve, their results imply a critical density $\Sigma_{crit}(M_\odot\,pc^{-2}) = 0.69 \times 0.59 \times V_{rot}/R(kpc)$. From Bell & de Jong (2001) we take a mean relation for disk galaxies $V_{rot} = 131 \times M_{10}^{0.23}$, where M_{10} is the stellar mass in units of $10^{10}\,M_\odot$, giving us the critical density as a function of galactic radius of $\Sigma_{crit}(M_\odot\,pc^{-2}) = 53.3\,M_{10}^{0.23}/R(kpc)$. The star formation rates below the critical density are not well determined. They are not zero: observations show that parts of galaxies below the critical density typically have small, isolated star-forming regions. For lack of a better specification, we shall assume that below the critical density the SFR is 0.1 times the value predicted by the Schmidt–Kennicutt Law.

This more complete model is also shown in Figure 13 and it is is in much better agreement with the observations. There is now a distinct main sequence and a large group of quiescent galaxies with sSFRs about an order of magnitude lower than the main sequence. The gas to stellar mass ratio now flattens out at the location of the quiescent galaxies, with values of the gas to star formation ratio about a factor of five higher than on
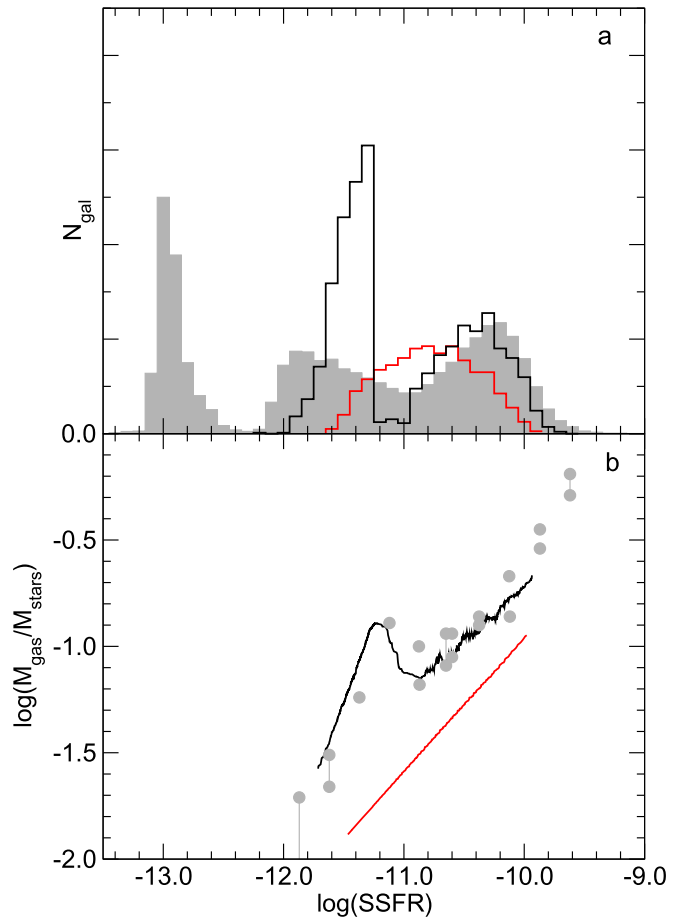
Figure 13. Comparison of properties of galaxies in the mass range $10.0 \leqslant \log$ (mass) < 11.0 with the predictions of a simple model of galaxy evolution. (a) Distribution of sSFR; gray area—observations, red curve model evolution without disk stability cutoff in SFR, black curve—model evolution with disk stability cutoff. (b) Median H I gas-to-stellar mass ratio vs. sSFR. Gray points —observations, red points—model without disk stability cutoff, black points— model with disk stability cutoff.

the main sequence. In fact, even the bump in gas-to-mass at log (sSFR) ~ -11.1 is reproduced. The reasons for this different behavior is explained in Figure 14, which presents the SFR histories of a sampling of galaxies of varying mass, t_0, and t_1 values, with and without stability quenching. Compared to models without a disk instability threshold, the star formation in models with a threshold drops more rapidly, as less and less of the galaxy is above the density threshold. Once all of the galaxy is below the threshold, the global star formation efficiency stops falling, the gas consumption rate becomes very low, and the star formation rate drops very slowly. Galaxies move slowly in the mass–sSFR plane and pile up near the locus at which they made the transition. Although gas density in the disk drops with radius, so does the critical density, so the entire galaxy makes the transition over a relatively short timescale. *And note that, again, a wide range of randomly selected star formation histories has produced a narrow main sequence.*

The agreement of model and observations in Figure 13 is, in fact, quite remarkable, given how simple our model is. It must be stressed that no tweaking of parameters has been done; we have taken star formation behavior straight from Kennicutt (1998) and Martin & Kennicutt (2001), and galaxy structure straight from Simard et al. (2011). This strongly suggests that no additional astrophysics and no additional gas flows are
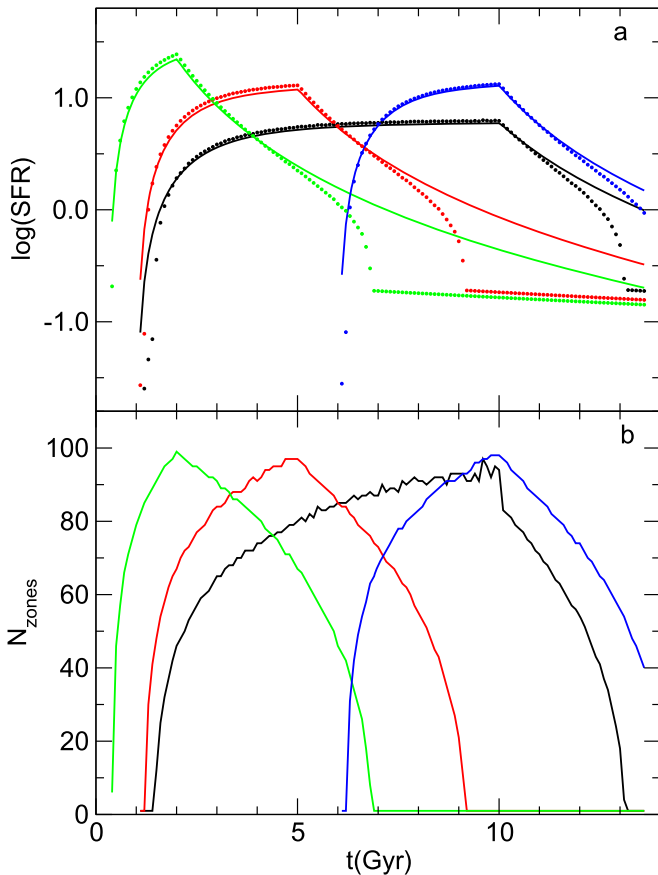
Figure 14. Star formation histories of sample galaxies in our toy model. (a) Star formation vs. time; solid lines are models without a disk instability threshold, circles are the same models with threshold. Parameters t_0, t_1 of the models are: green—3×10^8, 3×10^9, red—1×10^9, 5×10^9, black—1×10^9, 1×10^{10}, blue—6×10^9, 1×10^{10}. (b) Number of 100 pc radial zones with gas density above the instability threshold vs. time. Color coding is the same as in (a).

necessary to move galaxies from the main sequence to the quiescent state. By itself, the rather small dispersion in gas-to-mass ratios seen at a given sSFR in Figure 10 implies that the mass of cold gas observed by ALFALFA and GASS is equal to the mass of star-forming gas; little has been missed and little is beyond the star-forming region. The agreement of model and observations further implies that this gas mass is neither increased by significant inflows not depleted by outflows, *at least during the main sequence to quiescent transition* (more on this soon.) The meaning of the quiescent population is now clear: *quiescent galaxies are those in which the density of cold disk gas is below the gas disk instability threshold.* All of the evidence presented in this paper is consistent, then, with the hypothesis that the evolution of disk galaxies away from the main sequence is driven by the depletion of gas due to star formation. The rate of evolution and the appearance of the galaxies is governed by the Schmidt–Kennicutt Law, as modified by an instability threshold.

We have now solved the problem of the quiescent galaxies, but at the expense of raising another: if galaxy evolution due to star formation almost stops at, say, log sSFR ~ -11.2, how do galaxies make their way to lower values of sSFR, and how do they deplete their gas and enter the passive state? Two possibilities seem obvious: either (1) some galaxies, either contemporaneous with those entering the quiescent state or at

an earlier epoch, somehow avoided the drop in star formation rate and managed to turn their remaining gas into stars, or (2) another process is active, which removes the remnant gas by other means. Possibility 1 seems unlikely, at least for disk galaxies. In a following paper (Oemler et al. in preparation) we will show that disk structure seems almost constant below log (sSFR) < -11.0, so that there is no reason to think that gas in the now-passive disks experienced very different conditions than those in quiescent disks today. Ellipticals are, of course, a different matter: It is well known that bulge-dominated galaxies are more prevalent among passive galaxies, and our toy model has no relevance to bulge formation. However, bulge-dominated galaxies comprise at most 30% of the passive population, so different star formation astrophysics in bulges cannot be more than part of the answer.

Possibility 2 seems more promising, and many mechanisms are known that can expel gas from galaxies. The strengths of many are proportional to the star formation rate and are unlikely to be effective at the very low SFRs of the quiescent galaxies, but not all have this limitation. Some Type I supernovae occur well after the cessation of star formation, as do winds from AGB stars. AGNs may as well, although it is not clear how important AGNs are in galaxies with small bulges. Any such mechanism must be able to explain Figure 9, which plotted over the entire observed range of mass and environment, the ratios of main sequence to other galaxies, and the ratio of quiescent to passive galaxies. These quantities are independent of each other, but there is a quite tight correlation between the two, at almost all values of mass and density. Thus, if we try to invoke separate explanations for the transformation of main-sequence galaxies into quiescent objects and for the transformation of quiescent into passive objects, we must contrive a tight connection between the two processes.

Fortunately, there is a natural connection. Comparison of the model and observed sSFR distributions in Figure 13 implies that the transformation process we are seeking operates on a fairly long timescale, longer than a few Gyr but shorter than a few tens of Gyr. If it were as short as the former, all quiescent galaxies at log(sSFR) ~ -11.2 would have been quickly transformed into quenched objects. If it were as long as the latter, all would still be at log(sSFR) ~ -11.2 rather than spread all the way down to the passive region. In our model, the evolutionary rate and present state of a galaxy depends mostly on the epoch at which inflow ends. If certain environments and masses skew this epoch toward earlier values, more galaxies will have entered the quiescent state by now, *and, on average, they will have done so at an earlier time.* Thus, there will have been more time for the slowly working quiescent to passive transformation process to work, and more will have made the transition (see Kelson et al. 2016, which come to similar conclusions from a different direction.)

4.3. The Role of Environment

It is our contention that the post-main-sequence evolution of disk galaxies is driven by two intrinsic processes: the depletion of H I gas through star formation followed by the expulsion of the remaining gas, probably by the combined effects of stellar winds and supernovae. However, this intrinsic process only begins after an extrinsic event: the cessation of the net inflow of cold gas from outside. Now, it is possible, since it is the *net* inflow that matters, that this is an intrinsic effect, due to an

increase in outflows, perhaps driven by an AGN, rather than a cessation of inflow. However, unless such outflows were delicately balanced so as to only cancel the continuing inflows, rather than result in the rapid expulsion of all gas, such an event would lead to a much more rapid decline in star formation and a much more rapid evolution of the galaxy toward the passive state than is evidenced by the sSFR distribution in Figure 13.

Figure 8 confirms what has long been known: dense environments (and higher masses) push the galaxy population toward lower star formation rates. Given our model, these are, in fact, the trends one might expect. The environmental dependence on gas inflow was first proposed by LTC80, who noted that the observed star formation rates and gas content of spiral galaxies required continual infall of new gas if star formation was not to fade, and proposed that S0 galaxies were the product of the truncation of gas infall in dense environments. More recent models of a Λ cold dark universe support such an idea. For example, Dekel & Brinboim (2006) argued how the mass of the dark matter halo might govern the thermal properties of the infalling gas. Lower mass galaxies are fed by streams of cold gas, which can continue to feed star formation for extended epochs. In high-mass galaxies, the gas is shock heated to high temperatures at earlier times, after which it is more vulnerable to dispersal by winds generated by star formation and AGNs. Feldmann et al. (2011, F11) performed one of the first fine-scale numerical simulations of a large enough volume to simultaneously resolve the intrinsic processes of galaxies and also include a large enough volume to study the extrinsic processes driving evolution. They found that the evolutionary history of disk galaxies in a group are primarily driven by (a) mergers, which form the bulge component, (b) suppression of gas infall within the group environment, and (c) ram pressure stripping when galaxies pass through the group center. The stellar and gas content of the galaxies today depend on how long they have been in the group environment: those that entered first have evolved the most toward the passive state.

A significant role for ram pressure stripping of the disk gas is *not* consistent with our observations, since that would accelerate gas depletion and accelerate the transition of galaxies toward the passive state; nor is it consistent with the different bulge contents of main-sequence and passive galaxies shown in Figure 11. However, the environment in the F11 simulation is denser than that experienced by the average galaxy. Although perhaps half of all galaxies are in groups, meaning that they have at least one neighbor of comparable or larger mass, the typical group is significantly smaller than that studied by F11. Cen (2014) performed a larger-scale simulation of galaxies in their environments, containing 3000 galaxies in a considerably wider range of environments. He also found that ram pressure stripping is important, but only for removing the large-scale cold gas halos surrounding galaxies that resupply the disk. The subsequent evolution of the gas content of the disk is driven, as in LTC80, by star formation (see also Rafieferantsoa et al. 2015). We conclude, therefore, that ram pressure stripping of gas disks, as originally proposed by Gunn & Gott (1972), will only be important for that small subset of galaxies living in the densest environments.

In our picture, the environmental dependence of galaxy stellar populations has two parallel components: the population of quiescent plus passive galaxies is driven by *how many* galaxies have had their outer gas halos removed sufficiently long ago for gas content to have fallen below the stability threshold, while the ratio of quiescent to passive galaxies is driven by *how early* the halos were removed. It is reasonable to expect, and consistent with the models of Feldmann et al. and Cen, that the two trends should go together.

5. Summary and Conclusions

Beginning with rates inferred from hydrogen recombination lines, we have recalibrated star formation rates based on a combination of near-UV plus mid-IR flux, taking account of the fact that even old stellar populations have some flux in each of these bands. Using this, we examined the reliability of the largest available set of star formation determinations, that of SDSS galaxies by B04, as later modified and applied to the SDSS DR7 data release. We showed that the B04-DR7 values are generally quite good, but with systematic problems at low star formation rates. However, combining recalibrated B04-DR7 values with rates derived from the near-UV versus g band colors, we demonstrated that we can reliably measure specific star formation rates down to $\log(\text{sSFR}) \sim -12$.

After dealing with selection effects, which bias optically selected galaxy samples against low sSFR objects, we constructed a sample of about 10^5 objects drawn from the B04-DR7 sample, which is biased in mass but unbiased in sSFR. This sample contains a very large number of galaxies with detected specific star formation rates well below that of the main sequence. The sSFR distribution of the sample suggests that the low sSFR objects might form a distinct set rather than the low tail of the main sequence, and we divide the sample into three subsets: *main sequence*, low sSFR objects, which we denote as *quiescent*, and *passive* objects with no detected star formation. We suspect that the passive and quiescent objects form a continuum, but since we are unable to resolve it we treat them as members of separate groups.

We use measures of the galaxies' environments from Tempel et al. (2012), determinations of disk and bulge mass from Mendel et al. (2014), and gas content from the ALFALFA and GASS surveys, and we find the following trends among these populations.

1. Averaged over all masses and environments, main-sequence, quiescent, and passive galaxies each comprise about one third of the total galaxy population.
2. Disk-dominated ($B/T < 0.2$) galaxies are found only among main-sequence galaxies, but few main-sequence galaxies are bulge-dominated ($B/T > 0.9$).
3. The fractions of main-sequence, quiescent, and passive galaxies are sensitive to environment and mass, main-sequence fractions falling and quiescent and passive fractions rising at higher mass and density
4. The mass and environment sensitivity of the three sSFR groups seem to depend on only one physical variable: the ratio of quiescent to passive galaxies is a tight function of the fraction of main-sequence galaxies.
5. There is a tight $\sigma \sim 0.3$ dex correlation of sSFR with gas content; compared to main-sequence galaxies, quiescent galaxies are overabundant in gas.

These trends place significant constraints on the histories of star formation in disk galaxies. We have shown, however, that one item—the existence of a tight correlation of mass with star formation rate, i.e., the main sequence—does *not* provide much constraint, and that any ensemble of star formation histories that satisfy two conditions—varying smoothly with time and

decreasing at the present epoch—will display such a "main sequence."

Recent work on the evolution of star formation has been dominated by one concept, that of the "quenching" of star formation. This is, perhaps, an unfortunate choice of terminology because "quench" is an ambiguous verb, which can be either transitive or intransitive, but is usually thought of as the former. Star formation quenches in a galaxy when star formation ceases, but that does not imply that it is quenched by an outside agency: the expulsion of gas by an AGN, the stripping of gas by ram pressure, or some other active force. The most basic reason why star formation ceases is that a galaxy runs out of gas, and the most basic reason why a galaxy runs out of gas is that it has turned all of it into stars. Unless provided with an endless new supply, that will happen to any galaxy, whether or not it is subjected to any additional gas removal process, as LTC80 noted long ago.

Multiple pieces of evidence presented above suggest that the evolution of disk galaxies, in almost every environment, is driven by nothing more than gas exhaustion. The lack of disk-dominated quiescent and passive galaxies rules out any galaxy histories—stripping for example—in which the cessation of star formation is unconnected to the processes which built the galaxy's structure. Furthermore, the tight correlation of gas content and star formation rate, combined with the existence of a very large population of quiescent galaxies requires that the process behind gas removal acts very slowly, much slower than either ram pressure stripping or AGN-driven gas expulsion are likely to work. Since both of these processes work best when the gas density is low; they should, once started, drive the gas content to zero, rather than to the low but still significant levels seen in the quiescent galaxies.

We have shown, using a simple but not unrealistic model for disk galaxies, that the properties of main sequence and quiescent galaxies are naturally explained by the observed dependence of star formation rate on the density of gas in the disk. The evolution off the main sequence is governed by the Schmidt–Kennicutt Law, and the pile up of galaxies in the quiescent region is the result of the depression of star formation rates when disk gas density falls below a critical level, possibly set by the Toomre disk stability criterion. The only thing needed to start this evolution is for the infall of new gas into the disk cease, or at least drop to such a low level that it is unable to replace the gas that is locked up into new stars.

In this picture, the evolution of disk galaxies is driven not by the (transitive) quenching of star formation due to some gas removal process, but rather by the (transitive) quenching of gas infall into disks, which precedes, by some billions of years, the (intransitive) quenching of star formation. The cutoff in gas infall provides a natural explanation for the environmental dependence of galaxy populations seen in Figure 8, since models show that such a cutoff tends to occur at earlier times in denser environments. The structure of disk galaxies present other challenges. If our model is correct, the correlation of bulge-to-disk ratio with sSFR, and therefore with disk evolutionary state implies a coherence between the bulge-building phase of galaxy evolution and the epoch at which gas infall ends. This may be so, but further consideration is beyond the scope of this paper.

Finally, we should comment on the connection between these findings and the log-normal model for star formation histories that we previously described (G13, Abramson et al.

2015, 2016). That model is characterized by star formation rates that peak at intermediate epochs and are characterized by two independent timescales. The star formation histories in Figure 14 share these characteristics, but not a precise log-normal shape. This is not surprising, for several reasons. The observations that G13 fit were unable to detect the low sSFR levels of the quiescent galaxies and they therefore did not include that phase in their evolution. Also, the shapes of the star formation histories that we have constructed in this paper obviously depend on our choice of infall histories; the tophat form that we have used is unlikely to be an accurate description of actual infall. We are confident that we could more closely duplicate log-normal histories by tuning the infall histories, but we see little to be gained by such an effort. Whether the star formation histories of galaxies are accurately or only approximately log-normal in form remains an open question, but the existence of several timescales for galaxy evolution appears certain.

Appendix
Calibrating Galaxy Star Formation Rates and Structure

A.1. Star Formation Rates

The largest published set of star formation rates for nearby galaxies comes from B04 and is based on the 3″ fiber spectroscopy from the Sloan Digital Sky Survey (York et al. 2000). B04 first used the observed emission line strengths to divide the galaxies into five spectral categories based on line strength and the likelihood that the spectrum is contaminated by an AGN. The spectral energy distributions of objects with detectable emission lines and no AGN component were fit to a grid of stellar population models with a range of metallicity, ionization properties, and dust content, from which the star formation rate was derived. The SFRs of all other objects were derived from the strength of the 4000 Å break, D4000, by an empirical relation between break strength and SFR. Since the 3″ fibers only sample a fraction of the typical galaxy, B04 apply empirically derived aperture corrections based on the color distributions of the galaxies in SDSS imaging.

Salim et al. (2007) derived star formation rates for a very similar sample of SDSS galaxies using ultraviolet and optical photometry and argued that the B04 SFRs of galaxies with no detected emission lines, which were based on the D4000 index, were systematically too high by several orders of magnitude. In response to this, Brinchmann and collaborators recalculated star formation rates, also basing them on the newer SDSS Data Release 7. We will use these values, which we denote as B04-DR7, in all of the following analysis.

Brinchmann et al. have probably done as careful and thorough a derivation of star formation rates as is possible from the SDSS data, but the reliability of the results is inevitably limited by the nature of that data: color distributions plus moderate S/N optical spectroscopy over a portion of the galaxy. As we shall see, the random errors in the B04-DR7 SFRs of vigorously star-forming galaxies are small, but the risk of systematic errors remain, particularly at the lower star formation rates that are our particular interest. To calibrate these possible errors we need independent, accurate star formation rates for a representative sample of the B04-DR7
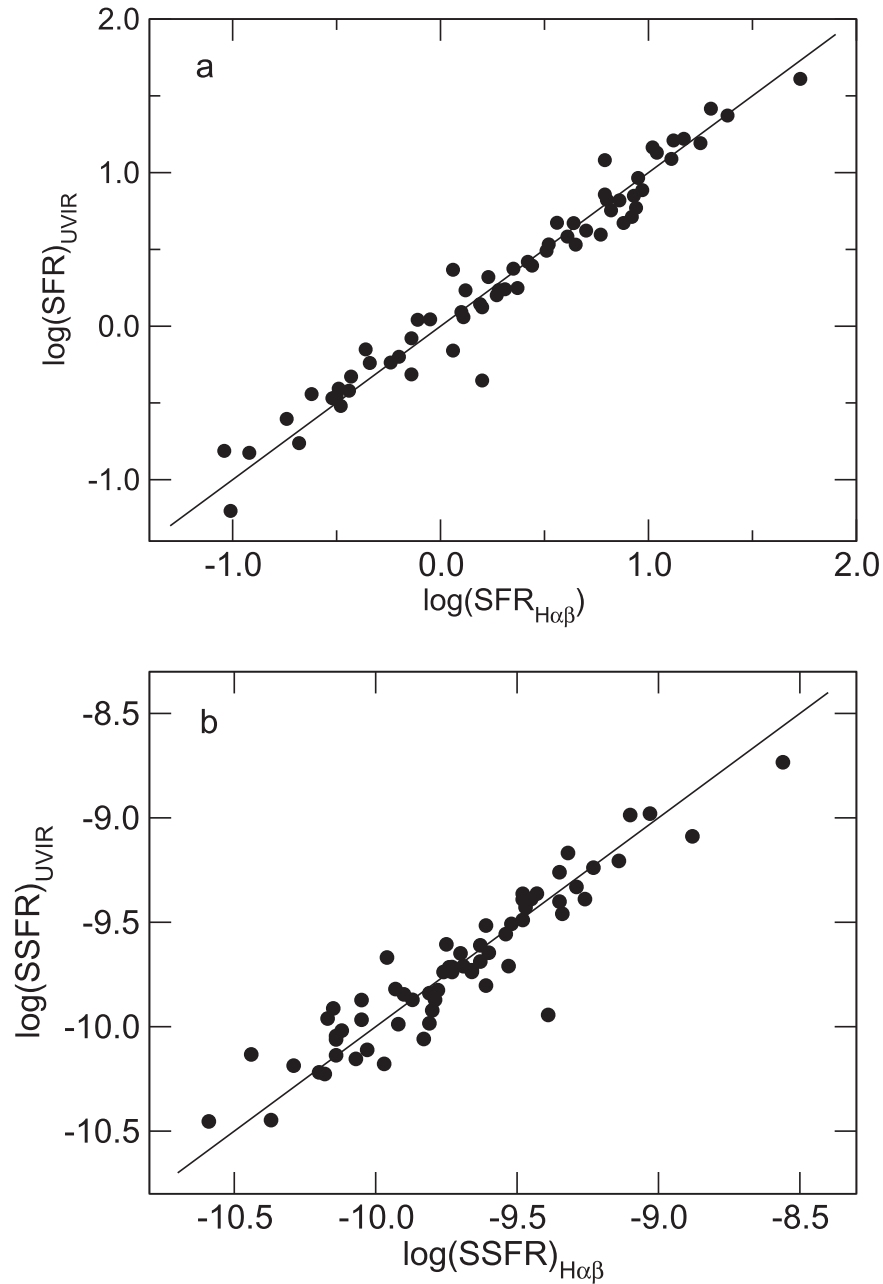
Figure 15. (Top) Star formation rates of MK06 sample galaxies calculated following Equation (4) vs. SFR from Balmer lines. (Bottom) Specific star formation rates for the same sample.

objects. Since aperture corrections are a significant worry, the sample must, among other things, be representative of the redshift distribution of the B04-DR7 sample, most of which lie in the range $0.01 \leqslant z \leqslant 0.20$.

All measures of star formation rates are indirect, but probably the best and least indirect are those based on the hydrogen recombination lines (Kennicutt 1998, K98 reviews all of the popular methods). Sufficiently accurate measures of at least two lines allow one to determine the extinction-corrected ionizing flux within H II regions, from which, with a few rather safe assumptions, the mass of young stars can be obtained. (Applying the method to entire galaxies is not free from error: if extinction within a galaxy is large and variable, the observed flux will come preferentially from the least-extincted regions and the average extinction correction will be underestimated.)

The most accurate emission line measurements of a suitable galaxy sample are probably those of Moustakas & Kennicutt 2006, MK06), which are derived from high signal-to-noise spectral scans over the entire face of a set of nearby galaxies. We derived Hα luminosities from the MK06 Hα and Hβ fluxes after correcting for Galactic extinction using Schlafly & Finkbeiner (2011). Star formation rates are obtained using Equation (2) of K98, but adjusted for a Kroupa (2001) IMF: $\mathrm{SFR}(M_\odot\,\mathrm{yr}^{-1}) = 5.6 \times 10^{-42} L_{\mathrm{H}\alpha}(\mathrm{erg\,s}^{-1})$.

These galaxies are not at all representative of the B04-DR7 sample: they are all at quite low redshift and are all vigorously star-forming, however, we can use them to calibrate another star formation measure that we can apply to a suitably large fraction of the B04-DR7 sample. The most suitable such measure is that based on a combination of ultraviolet and mid-infrared

flux. Because they are photometric rather than spectroscopic measures, these fluxes encompass the entire bodies of galaxies rather than the smaller regions usually sampled spectroscopically. Also, because the UV is a measure of that fraction of the (reprocessed) ionizing hot star radiation that escapes the galaxies, while the mid-IR is a measure of the fraction that is absorbed by and warms the galactic dust, a suitable combination should be (relatively) immune to extinction within the galaxy.

There are several ways of combining these two fluxes; we follow the method applied by Kennicutt et al. ([2009](#), K09) and simply assume that $SFR_{UVIR} = C_{IR}L_{IR} + C_{UV}L_{UV}$, where L_{IR} and L_{UV} are the luminosities in the UV and IR bands, solving for those values of C_{IR} and C_{UV}, which minimizes the scatter between SFR_{UVIR} and SFR_{Ha}.

We use the subset of normal galaxies from MK06, which is complied in Table 2 of K09. For the infrared flux we take the *IRAS* (Rice et al. [1988](#); Soifer et al. [1989](#), Moshir et al. [1990](#)) 25 μm fluxes quoted by MK06. For the UV we take fluxes in the near-UV band from the *GALEX* Nearby Galaxy Atlas (Gil de Paz et al. [2007](#)), corrected as before for Galactic extinction. The scatter between Hα and UV–IR derived star formation rates is minimized if we adapt

$$SFR_{UVIR} = 1.0 \times 10^{-43}(L_{25} + 0.75L_{NUV}). \tag{4}$$

The agreement between Hα and UV–IR star formation rates for the MK06 sample is presented in Figure [15](#)(a). The relation appears quite linear, with a scatter $\sigma(\log(SFR)) = 0.12$. For comparison, Whitaker et al. ([2012](#)) used a relation that, when converted to our units (K. Whitaker 2017, private communication), is almost identical: $SFR_{UVIR} = 1.0 \times 10^{-43}(L_{25} + 0.82L_{NUV})$.

To apply Equation ([4](#)) to the B04-DR7 sample, we take 22 μm magnitudes from the *WISE* All Sky Data Release (Wright et al. [2010](#); Cutri et al. [2012](#)), denoted as W4. A comparison of *WISE* magnitudes and *IRAS* fluxes for objects observed by both shows that $\log(F_{25})(Jy) = 0.4*(2.6 - W4)$. For k corrections we use the 24 μm k corrections from Rieke et al. ([2009](#)). Near-UV magnitudes are taken from the *GALEX* All Sky Imaging Survey Data Release 5 (Bianchi et al. [2011](#)). We will also make use of the 2MASS Ks magnitudes for our galaxies taken from the 2MASS Extended Source Catalog (Skrutskie et al. [2006](#)). We correct K and NUV magnitudes for Galactic extinction using Schlafly & Finkbeiner ([2011](#)) and apply k corrections from Chilingarian & Zolotukhin ([2012](#)).

Before proceeding with our recalibration of the B04-DR7 star formation rates, we must consider whether we can expect Equation ([4](#)) to be applicable at all levels of star formation, or more precisely, at all levels of *specific* star formation, since that is the quantity that we will be most interested in, and it is at very high or very low values of sSFR that Equation ([4](#)) is most likely to break down. Figure [15](#)(b) presents the relation for the MK06 sample; it is quite linear over the range sampled, but that range only encompasses the "main sequence." There is reason to expect the relation to fail at low levels of UV and IR flux. As Schiminovich et al. ([2007](#)) noted, old stellar populations as well as young populations contain hot stars—post-AGB stars, for example—which will produce a UV flux that is not indicative of star formation. The same is true in the mid-infrared, since most dust heating comes from the same hot stars that produce the UV (Wang & Heckman [1996](#)). Given the

uncertainties in the hot star populations of old stellar populations, it is safest to estimate this effect empirically.

Figure [16](#) plots the distribution of two colors, NUV $- K$ and $K -$ W4, for B04-DR7 galaxies with $z < 0.015$ and well-detected W4. These two colors compare the UV and IR indicators of hot stars to the cool stellar component that dominates in the K band. There is a trend in the expected direction, but the distribution is very broad, presumably due to the effect of internal extinction on the NUV flux. Also plotted, as black points, is a set of galaxies that are expected to have minimal star formation: ellipticals in which the ATLAS3D survey (Young et al. [2011](#)) detected no molecular gas. With a few exceptions—which may be true star-forming galaxies—these points cluster tightly around the region NUV $- K = 8.5$, $K -$ W4 $= 0.85$. We take these values to represent the UV and IR emission due to old stars, and therefore can produce UV and IR magnitudes corrected for this contamination as

$$NUV - K < 8.5:$$
$$NUV_{corr} = -2.5\log(10^{-0.4NUV} - 10^{-0.4(K+8.5)}), \tag{5}$$

$$K - W4 > 0.85:$$
$$W4_{corr} = -2.5\log(10^{-0.4W4} - 10^{-0.4(K-0.85)}). \tag{6}$$

Beyond NUV $- K = 8.5$ and $K -$ W4 $= 0.85$, NUV_{corr} and $W4_{corr}$ are set to arbitrarily large values. From these we calculate UV and IR luminosities to which we apply Equation ([4](#)) and we compare, in Figure [17](#), specific star formation rates so derived with those of B04-DR7. For reasons we will discuss shortly, we limit the sample to objects with disk inclination angles (from Simard et al. [2011](#)) less that 60°. The solid line has

$$\log(sSFR)_{UVIR} = \log(sSFR)_{B04corr}$$
$$= 1.07 \log(sSFR)_{B04} + 0.64. \tag{7}$$

The scatter, $\sigma(\log(sSFR))$, about this line ranges from 0.18 at $\log(sSFR) = -10.0$ to 0.56 at $\log(sSFR) = -11.5$. Thus, the B04-DR7 star formation rates are quite good for vigorously star-forming galaxies, but deteriorate significantly at lower specific star formation rates. This is hardly surprising: many of the latter had no detected emission lines, and star formation rates were estimated from D4000.

This comparison with B04-DR7 is inadequate in one way: the depth of the *WISE* photometry in insufficient to span most of the redshift range of that sample. The median redshift of objects in Figure [17](#) is only 0.025, at which the 3″_ SDSS fibers only cover an area 3 kpc in diameter. Thus, Figure [17](#) provides a stringent test of random errors in the B04-DR7 extrapolations, but the limited redshift range is insensitive to systematic errors. To test for such errors we turn to the SWIRE survey (Lonsdale et al. [2003](#)), which used *Spitzer* to survey six small fields in the two galactic caps—three within the B04-DR7 area—to much greater depth. Intercomparison between the SWIRE 24 μm photometry and the *WISE* and *IRAS* photometry show that $F_{25}(IRAS) = 1.5F_{24}(SWIRE)$. We then apply Equations ([4](#))–([7](#)) to the data and compare the $B04_{corr}$ and UV–IR specific star formation rates versus redshift in Figure [18](#). Galaxies with $\log(sSFR)_{B04corr} > -11.0$, which have a smaller scatter, are shown as filled circles, others as open circles. There is no apparent trend with redshift, implying
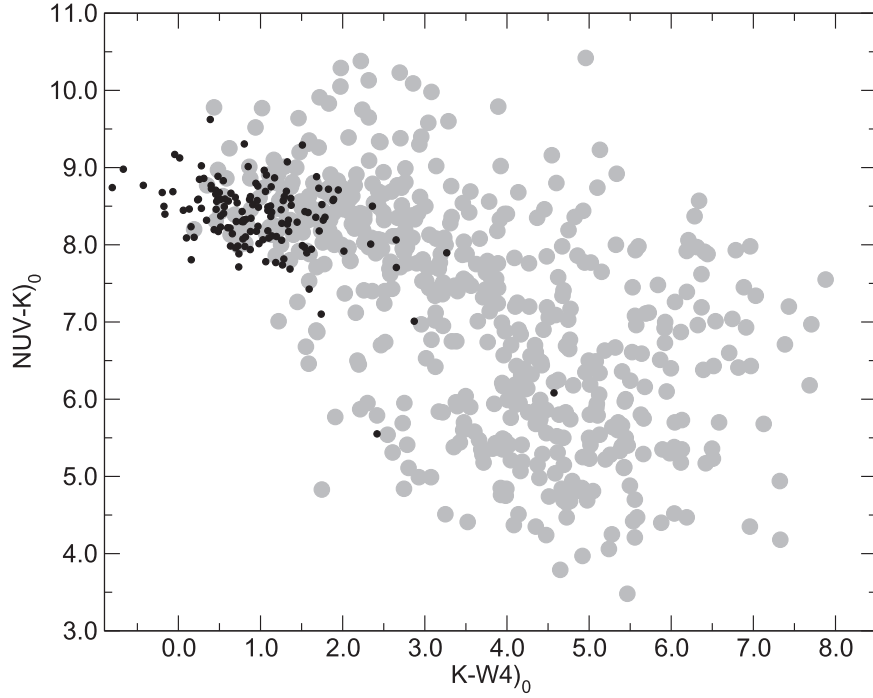
Figure 16. Distribution of galaxies in the $NUV - K$ vs. $K - W4$ plane. Gray points—all nearby B04-DR7 objects with well-detected *WISE* W4 magnitudes, black points—ATLAS3D ellipticals with no detected molecular gas.
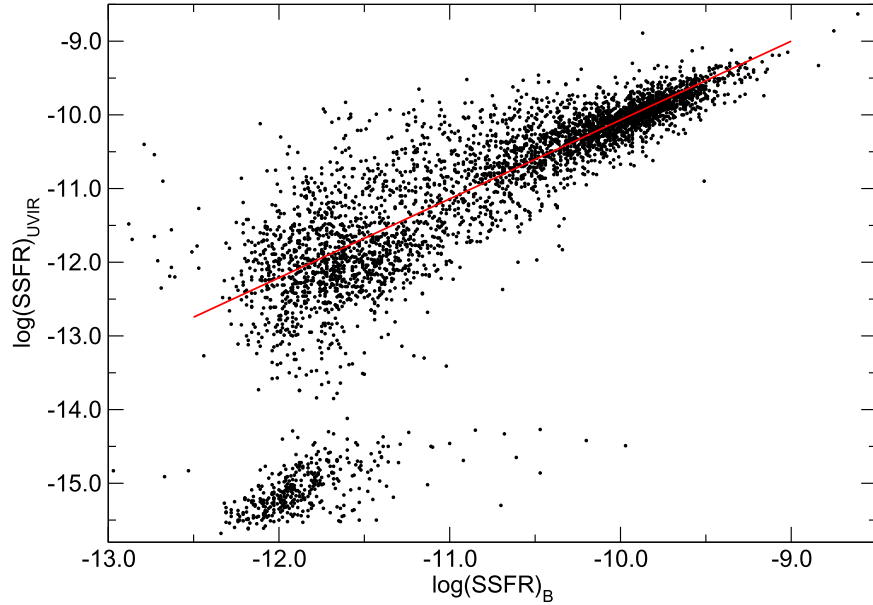

Figure 17. Comparison of specific star formation rates from B04-DR7 with those derived from UV+IR photometry. The straight line is the best fit, as described by Equation (4).

that the B04-DR7 aperture corrections have no systematic errors.

The above presentation confirms that once a small correction is applied, the B04-DR7 specific star formation rates are remarkably accurate and free of systematic errors. The sSFR values of vigorously star-forming galaxies are sufficiently accurate for our needs; however, random errors do increase significantly at lower levels of star formation. Ideally, we would like to keep $\sigma(\log(\mathrm{sSFR}))$ less than a few tenths at all detectable levels of star formation, but to achieve this we need

another accurate and independent measure of star formation. $\mathrm{sSFR_{UVIR}}$ would be ideal, but adequately deep mid-infrared photometry does not exist over most of the B04-DR7 sample volume. However, *GALEX* UV photometry does go deep enough and we shall examine one sSFR measure, based on $NUV - g$ colors. We take NUV magnitudes from *GALEX*, and g magnitudes from B04, correcting, as before, for Galactic extinction, k corrections, and the UV flux from old populations following Equation (5). Figure 19 presents the relation between $\log(\mathrm{sSFR})_{\mathrm{UVIR}}$ and $NUV - g)_0$ for the same sample used in
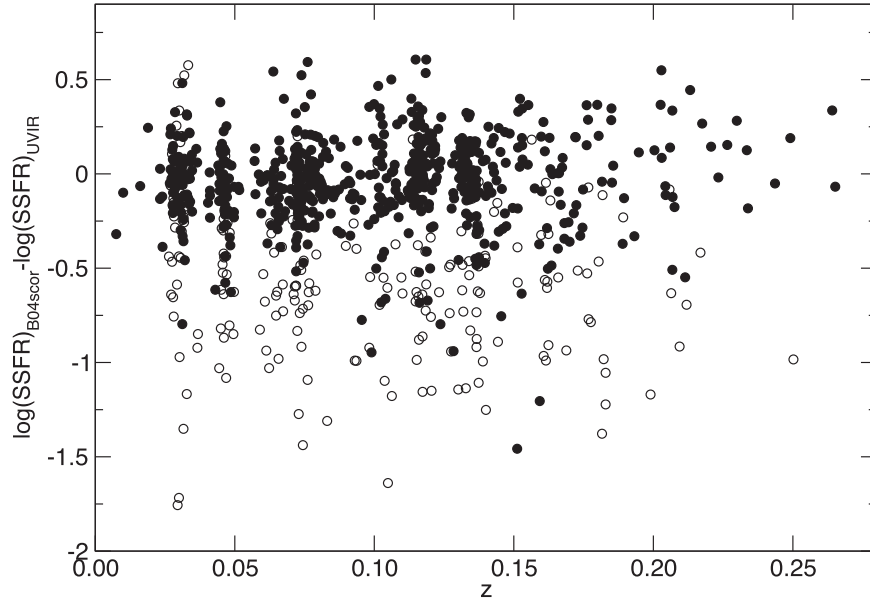
Figure 18. Scatter of $\log(\text{sSFR})_{\text{B04corr}} - \log(\text{sSFR})_{\text{UVIR}}$ vs. redshift. Filled circles are objects with $\log(\text{sSFR})_{\text{B04corr}} > -11.0$.
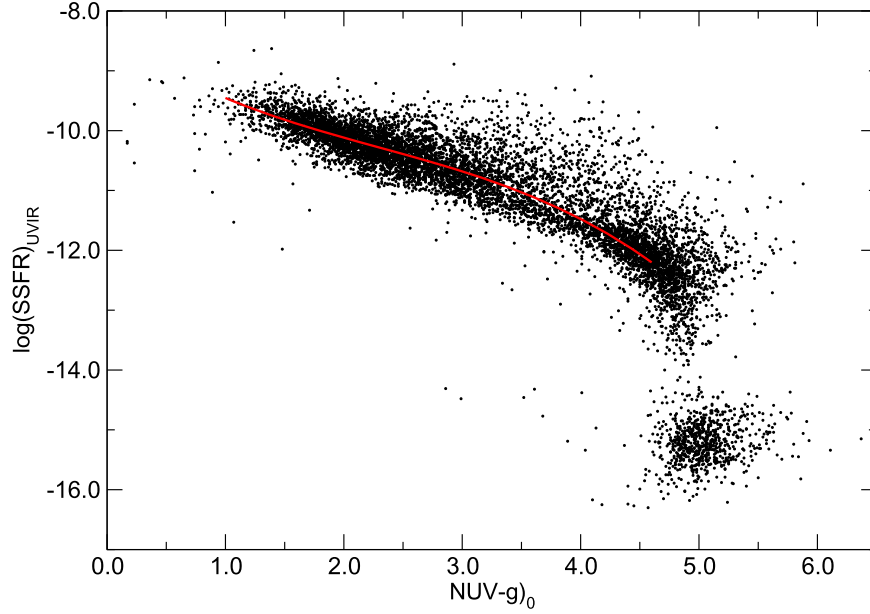

Figure 19. $\text{sSFR}_{\text{UVIR}}$ vs. $\text{NUV} - g$ color for the B04-DR7 sample. The red curve is the adapted relation described by Equation (8).

Figure 17. The solid line is a best fit for $\text{NUV} - g)_0 < 4.6$, and is of the form

$$\log(\text{sSFR})_{\text{UV}g} = -8.36 - 1.42(\text{NUV} - g) + 0.3809$$
$$\times (\text{NUV} - g)^2 - 0.05517(\text{NUV} - g)^3. \quad (8)$$

Given the sensitivity of UV flux to galactic extinction, it might seem puzzling how tight this correlation is. The reason, we surmise, is that both galactic star formation rate and dust content are well-correlated with gas content. The trend of observed $\text{NUV} - g$ color with sSFR is the sum of two factors: extinction and intrinsic $\text{NUV} - g$ color, both of which are well-correlated with sSFR.

We now define our sSFR measure

$$\log(\text{sSFR}) \equiv 0.5 * (\log(\text{sSFR})_{\text{B04corr}} + \log(\text{sSFR})_{\text{UV}g}) \quad (9)$$

and, in Figure 20, compare this with $\text{sSFR}_{\text{UVIR}}$. The two clouds of points to the left of $\log(\text{sSFR}) = -12.25$ include objects for which $\text{NUV} - g)_0 \geqslant 4.6$; those in the lower cloud also have either $\text{NUV} - K \geqslant 8.5$ or $K - W4 \leqslant 0.85$, or both. It is clear from this plot that we should assume that all values of $\log(\text{sSFR})$ less than -12.2 should be regarded as upper limits.

Next, we must revisit the issue of internal galactic extinction. B04 attempted to correct for extinction as part of their analysis, we have argued above that our fit of $\text{NUV} - g)_0$ versus $\text{sSFR}_{\text{UVIR}}$ automatically accounts for extinction and the IR +UV method is designed to be free of extinction effects. Thus, we would expect internal extinction to be unimportant, but
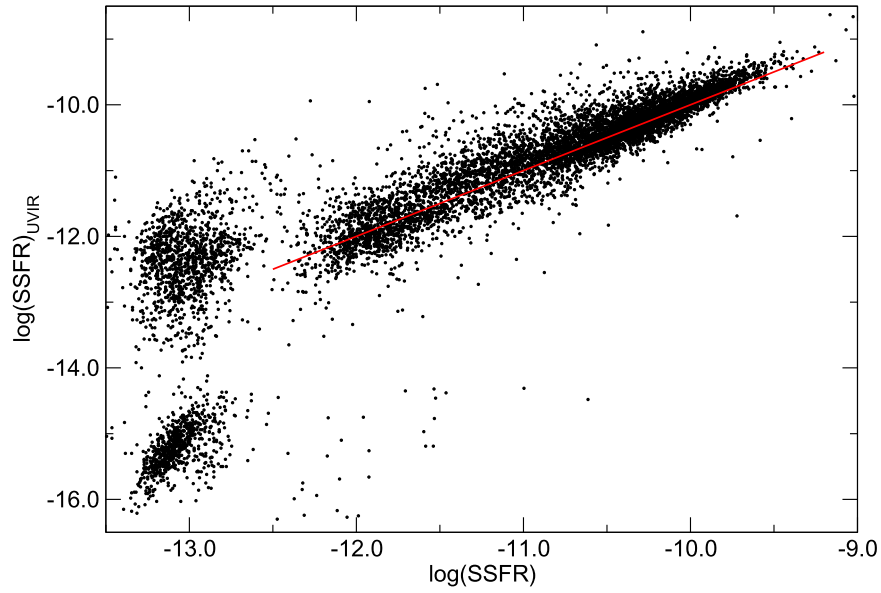
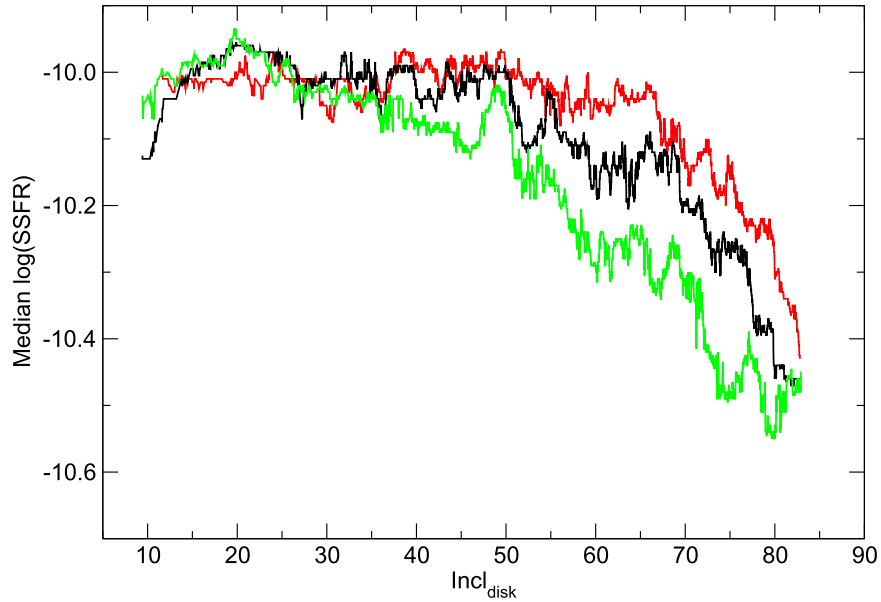**Figure 20.** Final sSFR values vs. sSFR$_{\mathrm{UVIR}}$.

Figure 21. Variation with disk inclination angle of the median sSFR of objects with log(sSFR) $\leqslant$ 11.0. Red—corrected B04$_{\mathrm{corr}}$ values, black—UV–IR values, green—UVg values.

Figure 21 shows that this is not true. For the galaxy sample used in previous figures, we plot the median value of sSFR versus disk inclination angle for objects with log(sSFR) $\leqslant$ -11.0. It appears that none of the methods properly account for extinction. B04-DR7 does the best job and NUV $-$ g color does the worst, but even the IR+UV method has serious extinction problems. It is easy to understand why this is so: the sum of IR and UV flux may *in the mean* account for all hot star ionizing flux, but only in the mean. The reradiation of absorbed UV flux by dust grains is a form of (energetic) scattering: flux is removed from the line of sight and is reradiated isotropically. Thus, at high inclination angles more energy is removed from the line of sight in the UV than is returned to the line of sight in the IR, and Equation (4) will underestimate the total star formation rate. To correct for this, we fit the median of our final

sSFR measure:

$$\Delta(\log(\mathrm{sSFR})) = 6.78 \times 10^{-3} I_{\mathrm{disk}} - 1.863 \times 10^{-4} I_{\mathrm{disk}}^2$$
$$+ 2.7543 \times 10^{-8} I_{\mathrm{disk}}^4. \quad (10)$$

We cut our sample at $I_{\mathrm{disk}} = 85°$. to minimize the uncertainty from very large corrections and apply this correction to our sSFR values. The final scatter in log(sSFR)$_{uvir}$ at fixed log(sSFR) ranges from 0.13 at log(sSFR) $= -10.0$ to 0.16 at log(sSFR) $= -11.5$, quite satisfactorily small.

References

Abell, G. O. 1965, ARA&A, 3, 1
Abramson, L. E., Gladders, M. D., Dressler, A., et al. 2015, ApJL, 801, L12
Abramson, L. E., Gladders, M. D., Dressler, A., et al. 2016, arXiv:1604.00016

Albareti, F. D., Allende Prieto, C., Almeida, A., et al. 2017, arXiv:1608.02013
Allington-Smith, J. R., Ellis, R., Zirbel, E. L., & Oemler, A., Jr. 1993, ApJ, 404, 521
Baade, W. 1951, POMic, 10, 7
Bell, E. F., & de Jong, R. S. 2001, ApJ, 550, 212
Bianchi, L, Herald, J., Efremova, B., et al. 2011, Ap&SS, 335, 161
Bouché, N., Cresci, G., Davies, R., et al. 2007, ApJ, 671, 303
Brinchmann, J., Charlot, S., White, S. D. M., et al. 2004, MNRAS, 351, 1151
Butcher, H., & Oemler, A., Jr. 1978, ApJ, 219, 18
Byrd, G., & Valtonen, M. 1990, ApJ, 350, 89
Catinella, B., Schiminovich, D., Kauffmann, G., et al. 2010, MNRAS, 403, 683
Catinella, B., Schiminovich, D., Kauffmann, G., et al. 2012, A&A, 544, A65
Cen, R. 2014, ApJ, 781, 38
Chilingarian, I. V., & Zolotukhin, I. Y. 2012, MNRAS, 419, 1727
Cowie, L., Songaila, A., Hu, E., et al. 1996, AJ, 112, 839
Cutri, R. M., Wright, E. L., Conrow, T., et al. 2012, yCat, 2311
Daddi, E., Elbaz, D., Walter, F., et al. 2010, ApJL, 714, L118
Dekel, A., & Birnboim, Y. 2006, MNRAS, 368, 2
Dressler, A. 1980, ApJ, 236, 351
Dressler, A., & Abramson, L. 2015, in IAU Symp. 311, Galaxy Masses as Constraints of Formation Models, ed. M. Cappellari & S. Courteau (Cambridge: Cambridge Univ. Press)
Dressler, A., Kelson, D. D`., Abramson, L. È., et al. 2016, arXiv:1607.02143
Dressler, A., Oemler, A., Jr., Couch, W. J., et al. 1997, ApJ, 490, 577
Dressler, A., Smail, I., Poggianti, B. M., et al. 1999, ApJS, 122, 51
Dutton, A. A., van den Bosch, F. C., & Dekel, A. 2010, MNRAS, 405, 1690
Eales, S., de Vis, P., Smith, M. W. L., et al. 2017, MNRAS, 465, 3125
Elahi, P. J., Knebe, A., Pearce, F. R., et al. 2016, MNRAS, 458, 1096
Feldmann, R., Carollo, C. M., & Mayer, L. 2011, ApJ, 736, 88
Gil de Paz, A., Boissier, S., Madore, B., et al. 2007, ApJS, 173, 185
Giovanelli, R., Haynes, M. P., Kent, B. R., et al. 2005, AJ, 130, 2598
Gladders, M. D., Oemler, A., Dressler, A., et al. 2013, ApJ, 770, 64
Gunn, J. E., & Gott, J. R., III 1972, ApJ, 176, 1
Haynes, M. P., Giovanelli, R., Martin, A. M., et al. 2011, AJ, 142, 170
Hopkins, P. F., Kereš, D., Oñorbe, J., et al. 2014, MNRAS, 445, 581
Hubble, E. P. 1926, ApJ, 64, 321
Hubble, E. P. 1936, The Realm of the Nebulae (New Haven: Yale Univ. Press)
Kauffmann, G., Heckman, T. M., White, S. D. M., et al. 2003, MNRAS, 341, 33
Kelson, D. D., Benson, A. J., & Abramson, L. E. 2016, arXiv:1610.06566
Kennicutt, R. C. 1989, ApJ, 344, 685
Kennicutt, R. C., Jr. 1998, ARA&A, 36, 189
Kennicutt, R. C., Jr., Hao, C.-N., Calzetti, D., et al. 2009, ApJ, 703, 1672
Kroupa, P. 2001, MNRAS, 322, 231
Larson, R. B., Tinsley, B. M., & Caldwell, C. N. 1980, ApJ, 237, 692
Lonsdale, C. J., Smith, H. E., Rowan-Robinson, M., et al. 2003, PASP, 115, 897
Madau, P. 1998, ApJ, 498, 106
Martin, C. L., & Kennicutt, R. C., Jr. 2001, ApJ, 555, 301
McGee, S. L., Balogh, M. L., Wilman, D. J., et al. 2011, MNRAS, 413, 996
Mendel, J. T., Simard, L., Palmer, M., Ellison, S. L., & Patton, D. R. 2014, ApJS, 210, 3

Moore, B., Katz, N., Lake, G., Dressler, A., & Oemler, A., Jr. 1996, Natur, 379, 613
Moshir, M., Kopan, G., Conrow, T., et al. 1990, BAAS, 22, 1325
Moustakas, J., & Kennicutt, R. C., Jr. 2006, ApJS, 164, 81
Murante, G., Monaco, P., Borgani, S., et al. 2014, arXiv:1411.3671
Navarro, J. F., & Benz, W. 1991, ApJ, 380, 320
Noeske, K. G., Weiner, B. J., Faber, S. M., et al. 2007, ApJL, 660, L43
Oemler, A., Jr., Dressler, A., Gladders, M. G., et al. 2013, ApJ, 770, 63
Peng, Y.-j., Lilly, S. J., Kovač, K., et al. 2010, ApJ, 721, 193
Rafieferantsoa, M., Dave, R., Angles-Alcazar, D., et al. 2015, MNRAS, 453, 3980
Rice, W., Lonsdale, C. J., Soifer, B. T., et al. 1988, ApJS, 68, 91
Richstone, D. O., & Malumuth, E. M. 1983, ApJ, 268, 30
Rieke, G. H., Alonso-Herrero, A., Weiner, B. J., et al. 2009, ApJ, 692, 556
Rodríguez-Puebla, A., Primack, J. R., Behroozi, P., & Faber, S. M. 2016, MNRAS, 455, 2592
Saintonge, A., Kauffmann, G., Kramer, C., et al. 2011, MNRAS, 415, 32
Salim, S., Rich, R. M., Charlot, S., et al. 2007, ApJS, 173, 267
Sandage, A., & Visvanathan, N. 1978, ApJ, 225, 742
Scannapieco, C. 2012, AN, 333, 470
Schiminovich, D., Catinella, B., Kauffmann, G., et al. 2010, MNRAS, 408, 919
Schiminovich, D., Wyder, T. K., Martin, D. C., et al. 2007, ApJS, 173, 315
Schlafly, E. F., & Finkbeiner, D. P. 2011, ApJ, 737, 103
Schmidt, M. 1959, ApJ, 129, 243
Simard, L., Mendel, J. T., Patton, D. R., Ellison, S. L., & McConnachie, A. W. 2011, ApJS, 196, 11
Skrutskie, M. F., Cutri, R. M., Stiening, R., et al. 2006, AJ, 131, 1163
Soifer, B. T., Boehmer, L., Neugebauer, G., & Sanders, D. B. 1989, AJ, 98, 766
Sparre, M., Hayward, C. C., Springel, V., et al. 2015, MNRAS, 447, 3548
Speagle, J. S., Steinhardt, C. L., Capak, P. L., & Silverman, J. D. 2014, ApJS, 214, 15
Springob, C. M., Haynes, M. P., Giovanelli, R., & Kent, B. R. 2005, ApJS, 160, 149
Struck, C. 2006, in Astrophysics Update 2, ed. J. W. Mason (Heidelberg: Springer), 115
Tacchella, S., Dekel, A., Carollo, C. M., et al. 2016, MNRAS, 457, 2790
Tempel, E., Tago, E., & Liivamägi, L. J. 2012, A&A, 540, A106
Tojeiro, R., Masters, K. L., Richards, J., et al. 2013, MNRAS, 432, 359
Toomre, A. 1964, ApJ, 139, 1217
Wang, B., & Heckman, T. M. 1996, ApJ, 457, 645
Whitaker, K. E., van Dokkum, P. G., Brammer, G., & Franx, M. 2012, ApJL, 754, L29
White, S. D. M., & Frenk, C. S. 1991, ApJ, 379, 52
Wright, E. L., Eisenhardt, P. R. M., Mainzer, A. K., et al. 2010, AJ, 140, 1868
York, D. G., Adelman, J., Anderson, J. E., Jr., et al. 2000, AJ, 120, 1579
Young, L. M., Bureau, M., Davis, T. A., et al. 2011, MNRAS, 414, 940